© 2022. Published by The Company of Biologists Ltd | Development (2022) 149, dev199752. doi:10.1242/dev.199752

STEM CELLS AND REGENERATION

RESEARCH ARTICLE

Heterogeneous *pdgfrb*$^+$ cells regulate coronary vessel development and revascularization during heart regeneration

Subir Kapuria[1,¶], Haipeng Bai[1,2,§], Juancarlos Fierros[1,3,§], Ying Huang[1], Feiyang Ma[4], Tyler Yoshida[1,5], Antonio Aguayo[1], Fatma Kok[6,*], Katie M. Wiens[1,7], Joycelyn K. Yip[8], Megan L. McCain[8,9], Matteo Pellegrini[4], Mikiko Nagashima[10], Peter F. Hitchcock[10], Naoki Mochizuki[11], Nathan D. Lawson[6], Michael M. R. Harrison[1,‡,¶] and Ching-Ling Lien[1,12,¶]

ABSTRACT

Endothelial cells emerge from the atrioventricular canal to form coronary blood vessels in juvenile zebrafish hearts. We find that *pdgfrb* is first expressed in the epicardium around the atrioventricular canal and later becomes localized mainly in the mural cells. *pdgfrb* mutant fish show severe defects in mural cell recruitment and coronary vessel development. Single-cell RNA sequencing analyses identified *pdgfrb*$^+$ cells as epicardium-derived cells (EPDCs) and mural cells. Mural cells associated with coronary arteries also express *cxcl12b* and smooth muscle cell markers. Interestingly, these mural cells remain associated with coronary arteries even in the absence of Pdgfrβ, although smooth muscle gene expression is downregulated. We find that *pdgfrb* expression dynamically changes in EPDCs of regenerating hearts. Differential gene expression analyses of *pdgfrb*$^+$ EPDCs and mural cells suggest that they express genes that are important for regeneration after heart injuries. *mdka* was identified as a highly upregulated gene in *pdgfrb*$^+$ cells during heart regeneration. However, *pdgfrb* but not *mdka* mutants show defects in heart regeneration after amputation. Our results demonstrate that heterogeneous *pdgfrb*$^+$ cells are essential for coronary development and heart regeneration.

KEY WORDS: Coronary vessels, Mural cells, Epicardium, *pdgfrb*, Zebrafish

INTRODUCTION

Coronary heart disease is the leading cause of human mortality worldwide. Understanding the mechanisms of coronary vessel development and revascularization has thus drawn much attention in the hope of advancing the treatment of heart disease. In contrast to mammals, zebrafish is a well-established, genetically tractable model organism that shows remarkable regenerative capacity in the adult heart. Fast vascularization is essential for regeneration of damaged zebrafish hearts (Marin-Juez et al., 2016). The presence of well-structured coronary vasculature and ease of imaging the developing and adult hearts make zebrafish an ideal system for exploring cellular and molecular mechanisms of coronary vessel formation. We previously reported that the Cxcr4a-Cxcl12b chemokine axis guides newly emerged endothelial sprouts from the atrioventricular canal (AVC) to undergo angiogenesis and gradually cover the juvenile heart ventricle during development (Harrison et al., 2015). However, the cellular and molecular mechanisms that govern the maturation and maintenance of the developed coronary network remain unclear.

Mural cells (including both pericytes and smooth muscle cells) are a collection of diverse supporting cells that are recruited onto endothelial cells and cover the circulatory vessels as single or multiple cell layers. They regulate vessel development, stability, and physical functions such as vessel contractility (Armulik et al., 2011). Endothelial cells express Platelet-derived Growth Factor b (Pdgf-b) and its receptor β (Pdgfrβ) is expressed by mural cells; this signaling regulates mural cell recruitment onto endothelial cells (Armulik et al., 2005, 2011; Hellstrom et al., 1999; Lindahl et al., 1997; Lindblom et al., 2003; Winkler et al., 2010). Genetic disruption of *Pdgfb* or *Pdgfrb* significantly decreases mural cell coverage on vessels throughout the mouse embryo (Hellstrom et al., 1999). In the central nervous system (CNS), loss of mural cell coverage in the vasculature makes the blood vessels hyperplastic (significantly more endothelial cells per vessel), dilated, and susceptible to hemorrhage (Lindahl et al., 1997).

In mouse hearts, mural cells originate from epicardial (Cai et al., 2008; Mellgren et al., 2008) and endocardial (Chen et al., 2016) cells. During development, pericytes are recruited to microvessels and mature further to become smooth muscle cells on coronary arteries. Smooth muscle cell differentiation is induced with the

[1]Department of Surgery, The Saban Research Institute and Heart Institute of Children's Hospital Los Angeles, Los Angeles, CA 90027, USA. [2]Laboratory of Chemical Genomics, School of Chemical Biology & Biotechnology, Peking University Shenzhen Graduate School, Shenzhen 518055, People's Republic of China. [3]Department of Biology, California State University, San Bernardino, San Bernardino, CA 92407, USA. [4]Department of Molecular, Cell and Developmental Biology, College of Letters and Sciences, University of California Los Angeles, Los Angeles, CA 90095, USA. [5]Department of Biological Sciences, Dornsife College of Letters, Arts and Sciences, University of Southern California, Los Angeles, CA 90007, USA. [6]Department of Molecular, Cell, and Cancer Biology, University of Massachusetts Medical School, Worcester, MA 01605, USA. [7]Science Department, Bay Path University, Longmeadow, MA 01106, USA. [8]Laboratory for Living Systems Engineering, Department of Biomedical Engineering, USC Viterbi School of Engineering, University of Southern California, Los Angeles, CA 90089, USA. [9]Department of Stem Cell Biology and Regenerative Medicine, Keck School of Medicine, University of Southern California, Los Angeles, CA 90033, USA. [10]Department of Ophthalmology and Visual Sciences, University of Michigan, Ann Arbor, MI 48105, USA. [11]Department of Cell Biology, National Cerebral and Cardiovascular Center Research Institute, Osaka, 564-8565, Japan. [12]Department of Surgery, Keck School of Medicine, University of Southern California, Los Angeles, CA 90033, USA.

*Present address: Institute of Cancer and Genomic Sciences, College of Medical and Dental Sciences, University of Birmingham, Edgbaston, Birmingham B15 2TT, United Kingdom. ‡Present address: Cardiovascular Research Institute, Weill Cornell Medical College, New York, NY 10021, USA.

§These authors contributed equally to this work

¶Authors for correspondence (skapuria@chla.usc.edu; mrh4003@med.cornell.edu; clien@chla.usc.edu)

S.K., 0000-0003-1307-5653; H.B., 0000-0003-3082-3078; J.F., 0000-0002-9225-4379; T.Y., 0000-0003-2193-4817; F.K., 0000-0002-2956-1253; M.L.M., 0000-0003-1908-6783; M.P., 0000-0001-9355-9564; P.F.H., 0000-0001-9454-2684; N.M., 0000-0002-3938-9602; N.D.L., 0000-0001-7788-9619; M.M.R.H., 0000-0003-1703-9879; C.-L.L., 0000-0002-5100-9780

Handling Editor: Steve Wilson
Received 28 April 2021; Accepted 4 January 2022

Development (2022) 149, dev199752. doi:10.1242/dev.199752

commencement of blood flow through the arterial vessel, which in turn stimulates Notch activation in the pericytes (Volz et al., 2015). PDGFRβ signaling is essential for coronary smooth muscle development in both mouse and avian hearts (Mellgren et al., 2008; Smith et al., 2011; Van Den Akker et al., 2005, 2008) and pericytes are decreased in *Pdgfrb* null mice (Volz et al., 2015). It is not yet clear how diverse the cardiac mural cell populations are and how PDGFRβ signaling regulates different mural cell populations.

Here, we describe *pdgfrb* expression patterns and mutant phenotypes, and heterogeneity of *pdgfrb*$^{+}$ cells during zebrafish coronary vessel development and heart regeneration. We find a subpopulation of *pdgfrb*$^{+}$ mural cells associated with coronary arteries that also expresses *cxcl12b*. These *pdgfrb; cxcl12b* double-positive coronary arterial mural cells express markers of smooth muscle cells. Interestingly, these arterial mural cells remain associated with the coronary arteries whereas other (non-arterial) coronary vessels lose *pdgfrb*$^{+}$ mural cells in the *pdgfrb* mutant. Single-cell RNA sequencing (scRNAseq) analyses reveal decreased smooth muscle gene expression, suggesting differentiation defects in these coronary arterial mural cells of *pdgfrb* mutants. Using a novel fluidic device-based culture and live-imaging system, we have further demonstrated that *pdgfrb* expression changes dynamically in the epicardium-derived cells (EDPCs) and that pre-existing mural cells migrate with angiogenic endothelial cells during heart regeneration. scRNAseq further reveal distinct populations of *pdgfrb*$^{+}$ EDPCs and pre-existing mural cells, and differential gene expression analysis suggests that these cells might play important roles during heart regeneration. Furthermore, *pdgfrb* mutants show defects in mural cell association with coronary endothelial cells during heart regeneration; this severely compromises the regenerative response. We have identified *mdka* as one of the top differentially expressed genes in *pdgfrb*$^{+}$ cells during heart regeneration. However, *mdka* mutants do not show severe defects in heart regeneration after amputation. Our results suggest that heterogeneous *pdgfrb*$^{+}$ cells are essential for coronary development and heart regeneration.

RESULTS

pdgfrb expression and the origins of *pdgfrb*$^{+}$ mural cells in developing zebrafish heart

To characterize spatiotemporal expression patterns of *pdgfrb* in the developing zebrafish heart, we utilized a *pdgfrb:mCitrine* transgenic reporter (Vanhollebeke et al., 2015). *pdgfrb* expression was consistently observed in the bulbus arteriosus (BA) and around the AVC at the late larval stage [24 days post-fertilization (dpf), ∼7 mm in standard body length (SL)], before any coronary endothelial cells emerged (Fig. 1A). In early juvenile fish, *pdgfrb* expression spread along the AVC at 31 (∼10.5 mm SL) and 43 dpf (∼17 mm SL). The coronary endothelial cells [marked by *Tg(fli1a:DsRed)* in Fig. 1A″] emerged on the ventricle around 36-49 dpf (∼14-18 mm SL). At the late juvenile stage by 55-74 dpf, *pdgfrb* expression became localized in the mural cells accompanying the nascent coronary endothelial cells sprouting out from the AVC (Fig. 1A‴, Fig. S1A).

As growing coronary vessels covered the ventricle, mural cells remained associated with large and small coronary vessels (Fig. 1A‴). Throughout development, mural cell density remained greater on the coronary vessels closer to the AVC (defined as the area proximal to the AVC) than the growing end of the vessels (regions distal to the AVC) (Fig. 1B, Fig. S1A). The colocalization of *pdgfrb:mCitrine* and *tcf21:DsRed* (which marks epicardium) around the AVC at 33 dpf (Fig. S1B) suggests that the origins of *pdgfrb*$^{+}$ cells might be the epicardium. To confirm this, we performed lineage-tracing experiments using the *tcf21:CreERT2* line combined with *pdgfrb:Citrine* and the *ubi:Switch* reporter. We observed that 76.15% of *pdgfrb*$^{+}$ cells were co-labeled with mCherry, indicating that most *pdgfrb*$^{+}$ cells were derived from the *tcf21*$^{+}$ epicardial lineage (Fig. 1Ca-Cb′, white arrowheads in Cc-Cc″, Fig. S1C). 23.85% of *pdgfrb*$^{+}$ cells (Fig. S1C) were not co-labeled with mCherry, suggesting that either *CreER-loxP* recombination was not efficient in these cells or these *pdgfrb*$^{+}$ cells were derived from other sources (Fig. 1Cd). Furthermore, we observed *tcf21:CreERT2*-labeled cells that did not express *pdgfrb* (Fig. 1Cc-Cc″, blue arrowheads), consistent with the notion that epicardium can also contribute to other cell types, such as fibroblasts in zebrafish (Sanchez-Iranzo et al., 2018) and mice (Ivey et al., 2018).

Next, we investigated whether the appearance of *pdgfrb*-expressing mural cells depends on blood circulation through the developing coronary vessels. We performed coronary angiography using *Tg(pdgfrb:Citrine; fli1a:DsRed)* juvenile zebrafish. *pdgfrb:Citrine*$^{+}$ mural cells were observed at 43 dpf on nascent coronary vessel sprouts in the absence of blood flow (Fig. 1D). By 50 dpf, initiation of blood flow through major vessels was observed in some hearts. However, in these juvenile fish *pdgfrb:Citrine*$^{+}$ mural cells were already attached to the immature vessel plexus without any detectable blood circulation (Fig. 1D′). All major vessels had blood flow by 64 dpf (Fig. 1D″). These results indicated that blood flow is not necessary for *pdgfrb:Citrine*$^{+}$ mural cell association with coronary vessels.

Pdgfrβ regulates mural cell recruitment to the coronary vessels and is required for coronary vessel development

To determine the role of Pdgfrβ during zebrafish coronary vessel development, we examined *pdgfrb*^{um148} homozygous mutants (*pdgfrb*$^{-/-}$; Kok et al., 2015). Consistent with findings in *Pdgfrb* knockout mice (Lindahl et al., 1997), the brain vasculature of adult *pdgfrb*$^{-/-}$ fish became significantly dilated with reduced branching density and decreased mural cell association (Fig. S2A). We did not observe hemorrhage in the heart ventricle. In *pdgfrb*$^{-/-}$ and *pdgfrb* heterozygous (*pdgfrb*$^{+/-}$) mutants, coronary vessels did develop, although not as efficiently as in wild-type (WT; *pdgfrb*$^{+/+}$) fish. Both *pdgfrb*$^{-/-}$ and *pdgfrb*$^{+/-}$ ventricles had reduced coverage of coronary vessels at 98 dpf (Fig. 2A, Fig. S2B′). Unlike in *pdgfrb*$^{+/-}$ fish, in which coronary vessel development was delayed, these defects in coronary vessel coverage remained by 167 dpf in *pdgfrb*$^{-/-}$ homozygous mutants (hereafter referred to as *pdgfrb* mutants) (Fig. 2A,A′). This phenotype is consistent with what was reported recently using a different *pdgfrb*^{sa16389} allele (Ando et al., 2021). Isolated endothelial cells, which fail to form continuous vessel networks, were observed in *pdgfrb* mutants (Fig. 2A, Fig. S2B, asterisks). Mural cell association with small vessels decreased significantly, but association with some of the large vessels remained unaffected in the *pdgfrb* mutants (Fig. 2B,B′, Fig. S2C). Further analysis revealed that among all large vessels, narrow large vessels (i.e. coronary arteries; Harrison et al., 2015) maintained *pdgfrb*$^{+}$ mural cell association (Fig. 2B, Fig. S2C, white arrowhead), whereas the wide large vessels (vein-like) lost a significant number of *pdgfrb*$^{+}$ mural cells (Fig. 2B, Fig. S2C, yellow arrowhead). Interestingly, in contrast to brain vessels that became dilated (Fig. S2A), the diameter of both wide large vessels and coronary arteries significantly decreased in *pdgfrb* mutants (Fig. S2D), suggesting a potential spatiotemporally

Development (2022) 149, dev199752. doi:10.1242/dev.199752

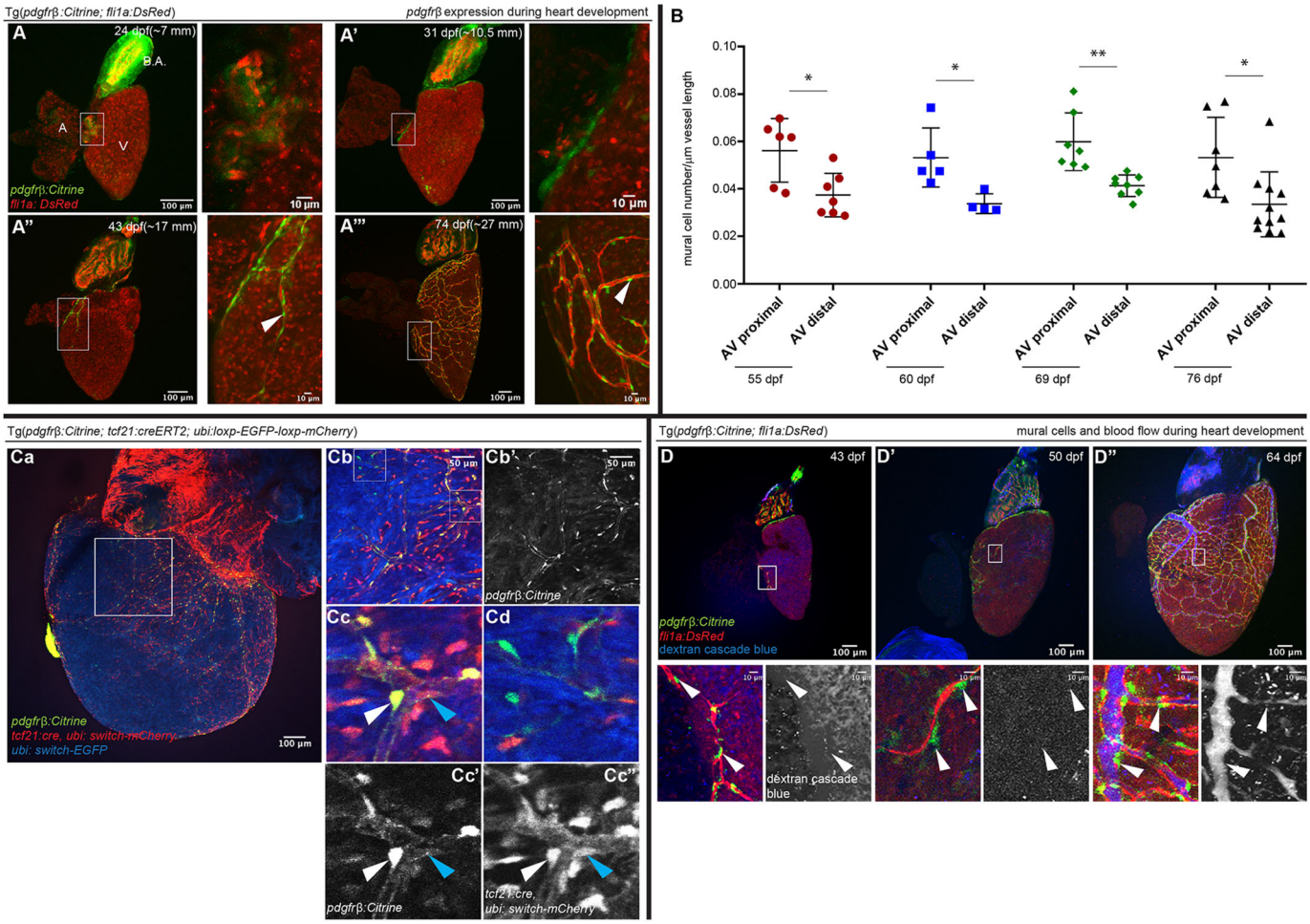

Fig. 1. *pdgfrb* expression and mural cell origin in the developing zebrafish heart. (A-A‴) *pdgfrb* expression during heart development at 24 dpf (~7 mm in body length; A), 31 dpf (~10.5 mm in body length; A′), 43 dpf (~17 mm in body length; A″) and 74 dpf (~27 mm in body length; A‴). The boxed areas are enlarged in the images to the right. Green, *pdgfrb:mCitrine*; red, coronary endothelial cells marked by *Tg(fli1a: DsRed)*. A, atrium; B.A. bulbus arteriosus; V, ventricle. *n*=5 hearts for each time point. (B) Quantification of *pdgfrb*$^{+}$ mural cell association. Mural cell number per μm of the coronary vessels proximal or distal to the AVC at different time points (55, 60, 69 and 76) dpf. Boxes in A indicate the vessels quantified as proximal to AVC. *n*=5-7 hearts for each time point. Error bars represent s.d. *$P\leq0.05$, **$P\leq0.01$ (unpaired, two-tailed *t*-test). (C-C‴) *tcf21*+ lineage traced cells contribute to *pdgfrb*+ mural cells. (Ca) Representative image of a *tcf21* lineage-traced fish at 87 dpf. *ubi:switch-GFP* (artificially colored blue) switches to *ubi:switch-mCherry* after recombination. *pdgfrb:Citrine*, green. (Cb-Cc) Enlarged views of the boxed areas in Ca and Cb. (Cc) *tcf21* lineage-traced (*mCherry*) cells co-labeled with *pdgfrb*$^{+}$ cells (white arrowhead) and *pdgfrb*$^{-}$ non-mural cell (blue arrowhead). Cc′ and Cc″ show single channels. (Cd) *pdgfrb*$^{+}$ cells (green) that are negative for the *tcf21* lineage. *n*=3. (D-D‴) Mural cell association around the coronary vessels does not depend on blood flow. Coronary angiography (dextran, blue) was performed to monitor blood flow at 43 (D), 50 (D′) and 64 (D″) dpf. White arrowheads indicate *pdgfrb*$^{+}$ mural cells in the images (enlarged views of the boxed areas above). *n*=5-6 hearts for each time point.

specific mechanism of blood vessel formation/maturation regulation by *pdgfrb*$^{+}$ mural cells. Taken together, these data suggest that different mechanisms might be utilized to regulate mural cell recruitment or maintenance along different subtypes of coronary vessels.

pdgfrb^{+}/*cxcl12b*$^{+}$-expressing cells covering the coronary arteries are smooth muscle like mural cells

We previously reported that epicardium-derived *cxcl12b:Citrine*-expressing mural cells surround *cxcr4a*$^{+}$ arterial endothelial cells (Harrison et al., 2015). Here, we also observed *pdgfrb*$^{+}$ cells covering coronary arteries (Fig. 2B, Fig. S2C,C′, narrow large vessels, white arrowheads). Therefore, we examined whether *cxcl12b:Citrine*$^{+}$ mural cells also express *pdgfrb:EGFP*. We observed that most (82.39%) of the mural cells on the coronary arteries express both *cxcl12b* and *pdgfrb* reporters (Fig. 3A′-A‴, blue arrowheads, 3A⁗). *pdgfrb:EGFP*$^{+}$ only (Fig. 3A′-A‴, green arrowheads) and *cxcl12b:mCitrine*$^{+}$ only (Fig. 3A′-A‴, red arrowheads) mural cells were less abundant on coronary arteries (12.88% and 4.73%, respectively) (Fig. 3A⁗).

We examined whether these *cxcl12b*$^{+}$ cells along the coronary artery are affected in *pdgfrb* mutants. Consistent with the finding using the *pdgfrb:EGFP* reporter (Fig. 2B, Fig. S2C), we found that *cxcl12b:Citrine*$^{+}$ (also *pdgfrb:EGFP*$^{+}$) mural cells remained associated with coronary arteries whereas other coronary vessels lost mural cells. Furthermore, the diameter of the coronary artery was significantly decreased in *pdgfrb* mutants (Fig. 3B). These results suggest that *pdgfrb*$^{+}$ mural cells are heterogeneous on the heart ventricle. The non-arterial mural cells express only *pdgfrb* and most of the mural cells on the coronary arteries are double-positive with *cxcl12b*. They also respond differently to the loss of *pdgfrb*.

To investigate further the gene expression signature in these *pdgfrb:EGFP*$^{+}$ and *cxcl12b:Citrine*$^{+}$ double-positive (*pdgfrb*$^{+}$/*cxcl12b*$^{+}$) mural cells and other *pdgfrb:EGFP*$^{+}$ only cells in WT controls versus *pdgfrb* mutants, we performed scRNAseq. We

Development (2022) 149, dev199752. doi:10.1242/dev.199752

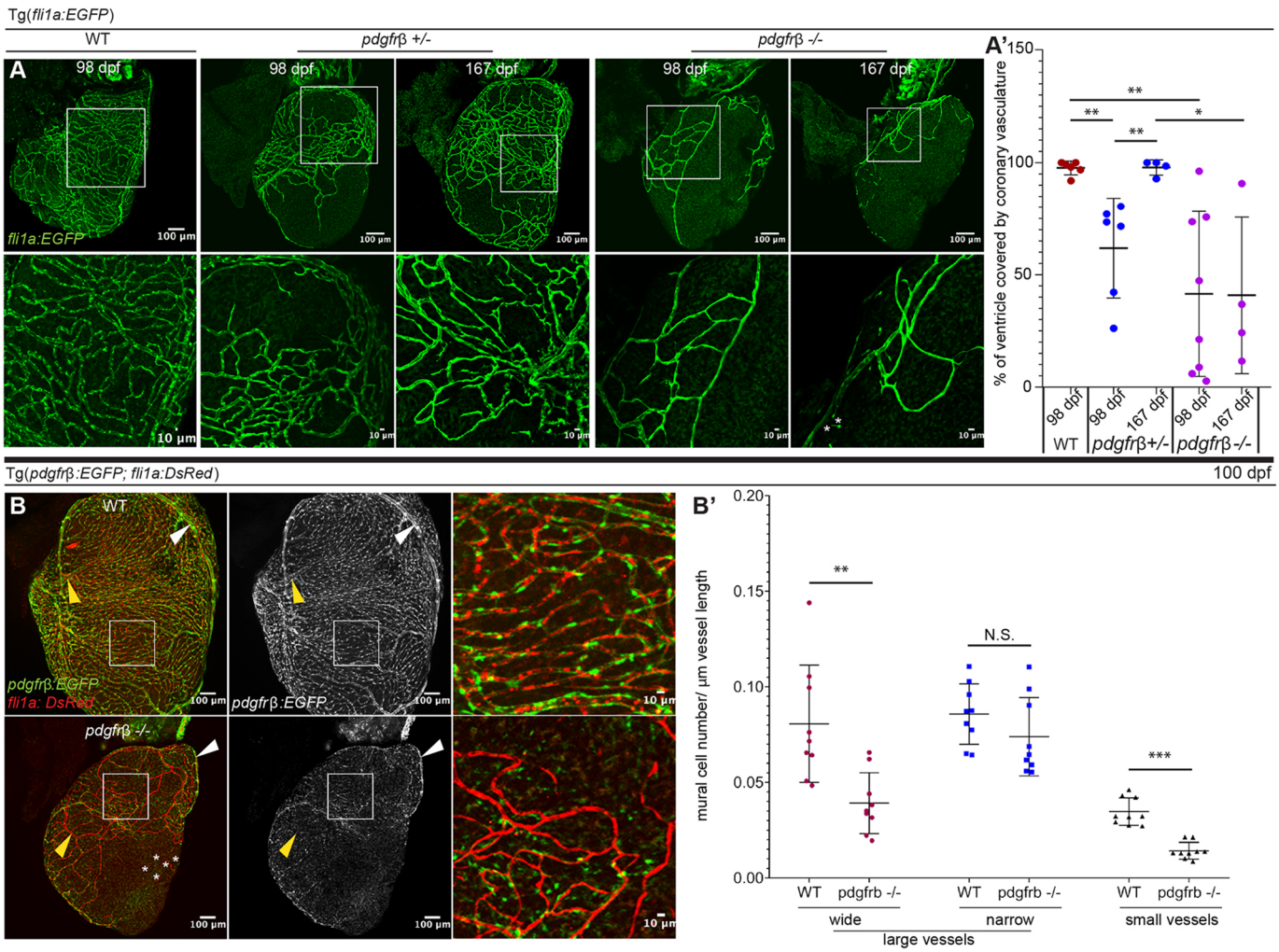

Fig. 2. Pdgfrβ regulates mural cell number, association, and development of the coronary vessels. (A,A′) Coronary vessel coverage of the ventricle. (A) Imaging of *fli1a:EGFP* in WT (*pdgfrb*$^{+/+}$), heterozygous (*pdgfrb*$^{+/-}$) and homozygous (*pdgfrb*$^{-/-}$) fish at 98 and 167 dpf. Asterisks indicate isolated endothelial cells. (A′) Quantification of coronary vessel coverage as a percentage of the ventricle area. *pdgfrb*$^{+/-}$ fish have decreased vessel coverage at 98 dpf (~61.8%, *n*=6 fish) but this recovered by 167 dpf (~97.85%, *n*=4 fish). *pdgfrb*$^{-/-}$ mutants have decreased vessel coverage at both 98 dpf (~41.45%, *n*=8 fish) and 167 dpf (~40.85%, *n*=4 fish) compared with WT (97.76%, *n*=7). Error bars represent s.d. **P*≤0.05, ***P*≤0.01 (one-way ANOVA). (B,B′) Mural cell association with different types of coronary vessels is affected differently in the *pdgfrb*$^{-/-}$ mutant. (B) Mural cell [*Tg(pdgfrb:EGFP)*] association with the small coronary vessels/capillaries [*Tg(fli1a:DsRed)*] is decreased at 100 dpf in *pdgfrb*$^{-/-}$ mutant heart. Mural cells are maintained around narrow, large (artery-like) vessels (white arrowheads), but the wider, large (vein-like) vessels (yellow arrowheads) lack mural cells. Asterisks indicate isolated endothelial cells. (B′) Quantification of mural cell recruitment on large and small coronary vessels. Mural cell number per µm vessel length on the narrow, large vessels is not significantly different between *pdgfrb*$^{+/+}$ and *pdgfrb*$^{-/-}$. Mural cell recruitment on the wide, large vessels and small coronary vessels is significantly decreased in *pdgfrb*$^{-/-}$ heart ventricles. *n*=3 vessels from each of 3-5 heart ventricles of *pdgfrb*$^{+/+}$ and *pdgfrb*$^{-/-}$ fish. Error bars represent s.d. ***P*≤0.01, ****P*≤0.001 (paired, two-tailed *t*-test). N.S., not significant (*P*>0.05).

sorted *pdgfrb:EGFP*$^{+}$ cells from *pdgfrb* mutants and sibling WT control fish by fluorescence-activated cell sorting (FACS) to enrich the mural cells, although different cell types (especially cardiomyocytes) were also collected, likely owing to autofluorescence (Fig. S3A,B,D, Table S1). Uniform manifold approximation and projection (UMAP) analysis revealed that the *pdgfrb*$^{+}$ and *egfp*$^{+}$ cells are mainly in clusters 3 and 6, whereas *cxcl12b*$^{+}$ cells are specifically in cluster 6. Furthermore, more cells expressed *egfp* transcripts at a higher level in cluster 6 (Fig. 3C, Fig. S3C). Differential gene expression analyses showed that the epicardial markers *tcf21* and *tbx18* are specifically found in cluster 3, suggesting that this cluster consists of epicardium and EPDCs. Cells in cluster 6 expressed more mural cell and smooth muscle cell markers (*acta2*, *myh11a*, *tagln*) (Fig. 3C′, Fig. S3C, Table S2). Furthermore, more cells in cluster 6 express higher *notch3*, which regulates vascular pericyte differentiation into smooth muscle cells (Volz et al., 2015) (Fig. 3C′, Fig. S3C′). Among other established mural cell markers (He et al., 2016; Whitesell et al., 2019), *rgs5a* and *cd248a* as well as a new marker, *ndufa4l2a*, were expressed in cluster 6 (Fig. 3C′) whereas *kcne4* was expressed in both clusters (Fig. 3C, Fig. S3C). Other brain pericyte markers, *abcc9*, *desma*, *cspg4*, *anpepa* (He et al., 2016), showed minimal expression in very few cells, indicating overall heterogeneity of the coronary mural cell population and their differences from brain mural cells. Furthermore, these data suggest that cluster 6 is likely composed of coronary mural cells. We validated expression of some of these mural cell markers by performing RT-PCR. The smooth muscle cell marker *acta2* showed increased expression in the *pdgfrb:EGFP* high cells, which likely represent the *cxcl12b*$^{+}$/*pdgfrb*$^{+}$ cells (Fig. 3C‴, Fig. S4). Because these cluster 6 mural cells express

Development (2022) 149, dev199752. doi:10.1242/dev.199752

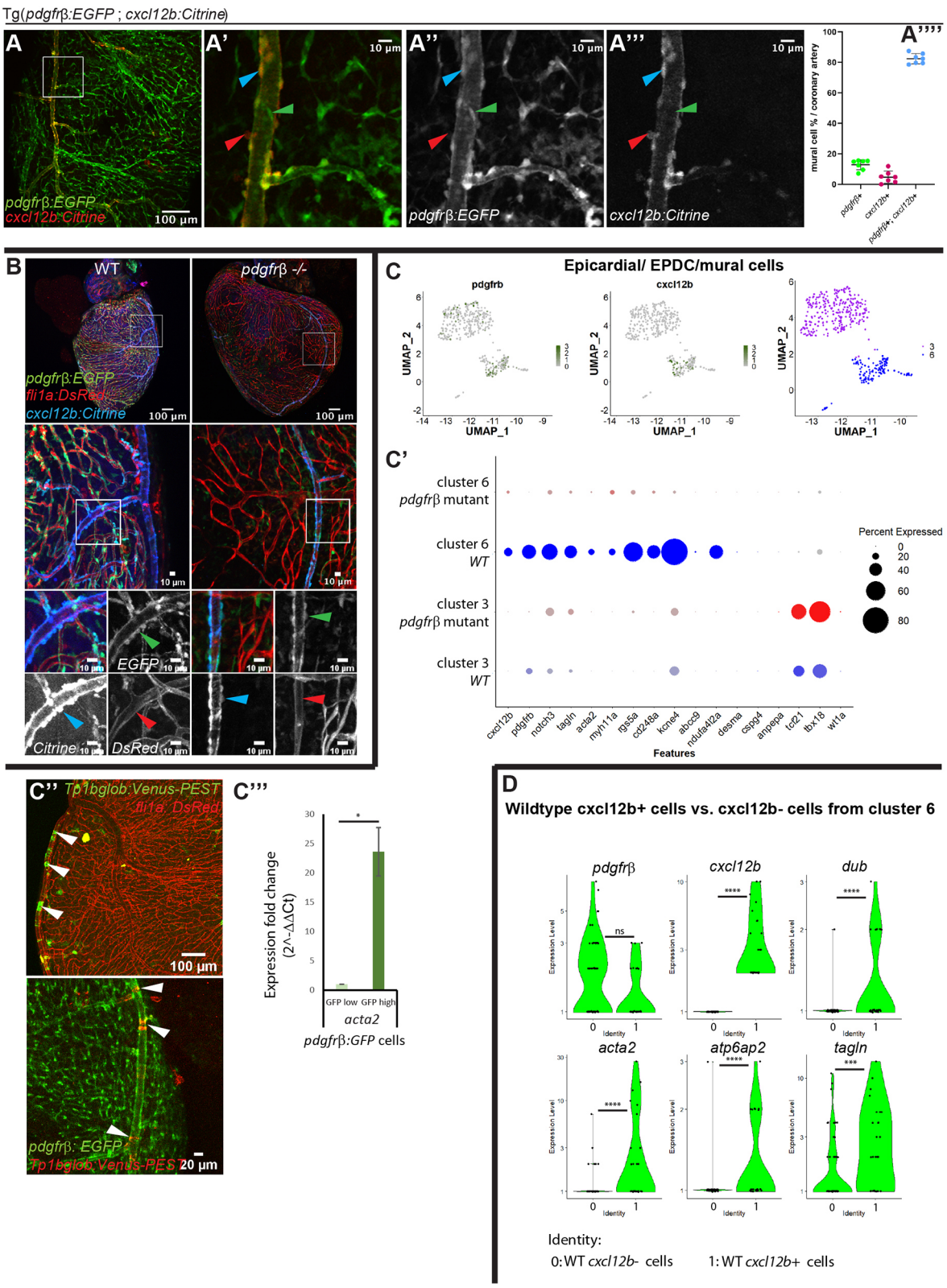

Fig. 3. See next page for legend.

notch 3, we determined Notch activity using the *Tp1bglb:Venus-PEST* reporter (Ninov et al., 2012) and found that the coronary arterial mural cells show high Notch activity (Fig. 3C″, white arrowheads). To characterize the arterial mural cells further, we selected *cxcl12b*$^{+}$ cells from cluster 6 and compared them with *cxcl12b*$^{-}$ (*pdgfrb*$^{+}$ only) cells. Differential gene expression analysis (Table S3) showed significantly higher smooth muscle marker gene (*acta2*, *tagln*) expression in the *cxcl12b*$^{+}$ cells, indicating that the coronary arterial mural cells are smooth muscle-like cells (Fig. 3D).

Development (2022) 149, dev199752. doi:10.1242/dev.199752

Fig. 3. *pdgfrb*$^{+}$;*cxcl12b*$^{+}$ arterial mural cells are smooth muscle-like and they remain associated with endothelial cells in the *pdgfrb* mutant. (A-A‴) The majority of the *pdgfrb*$^{+}$ mural cells express *cxcl12b* on the large, narrow vessels (coronary artery). (A-A‴). On the main trunk of the coronary artery, most *pdgfrb:EGFP*$^{+}$ mural cells (green) express *cxcl12b:Citrine* (blue arrowheads). A few mural cells only express *pdgfrb* (green arrowheads) or *cxcl12b* (red arrowheads). *cxcl12b* expression in the *pdgfrb*$^{+}$ mural cells gradually decrease on the branches away from the main coronary artery (A‴). A′-A‴ show enlarged views of the boxed area in A. (A‴) Quantification of *pdgfrb*$^{+}$;*cxcl12b*$^{+}$ (~82.4% of the mural cells on the coronary artery), *pdgfrb*$^{+}$ only (~12.9%) and *cxcl12b*$^{+}$ only (~4.7%) mural cells (*n*=5 hearts, 1-2 coronary arteries in each heart, 20× confocal images used for quantification). (B) In *pdgfrb*$^{-/-}$, *pdgfrb:EGFP*- and *cxcl12b:Citrine*-expressing mural cells remain associated with the coronary artery whereas other vessels lose mural cell association. Boxed areas are enlarged and shown as single-channel images beneath. (C-C‴) Differentially expressed genes between *pdgfrb* mutant and WT in cluster 3 (EPDC) and cluster 6 (mural cell). (C) FACS-isolated *pdgfrb:EGFP*$^{+}$ EPDCs and mural cells form two distinct clusters. The UMAP plot shows that cells in both clusters express *pdgfrb* and only one cluster expresses *cxcl12b*. (C′) Dot plot showing differentially expressed smooth muscle cell (*tagln*, *acta2*, *myh11a*), mural cell (*pdgfrb*, *notch3 rgs5a*, *cd248a*, *kcne4*, *ndufa4l2a*), epicardial (*tcf21*, *tbx18*) and *cxcl12* genes in cluster 3 and cluster 6 of *pdgfrb* mutant and WT. Differentially expressed genes were determined with minimum percentage expression cut-off=0.1 and minimum average log fold change=0.25, adjusted *P*-value≤0.001 comparing cluster 6 versus cluster 3 and *P*-value≤0.05 for *pdgfrb*, *notch3*, *tagln*, *rgs5a*, *cd248a* and *kcne4* comparing *pdgfrb* mutants and WT. (C″) Notch activities in coronary arterial mural cells, reflecting *nocth3* expression (white arrowheads). (C‴) qRT-PCR of *acta2* in GFP high (*pdgfrb*$^{+}$; *cxcl12b*$^{+}$) versus GFP low (*pdgfrb*$^{+}$ only) cells. **P*≤0.05 [one-sample (one-tailed) *t*-test]. (D) Violin plots of differentially expressed genes in WT *cxcl12b*$^{+}$ cells compared with *cxcl12b*$^{-}$ cells of cluster 6. 0=WT *cxcl12b*$^{-}$ cells, 1=WT *cxcl12b*$^{+}$ cells (average log fold change>0.8 except for *pdgfrb*$^{+}$). ****P*≤0.001, *****P*≤0.0001 (non-parametric Wilcoxon rank sum test). N.S., not significant (*P*>0.05).

In the *pdgfrb* mutant (*pdgfrb*$^{-/-}$), cluster 6 was most affected compared with other cell clusters (Fig. S5A). Cluster 6 contains ~11% of all WT cells and only ~2% of all *pdgfrb*$^{-/-}$ cells (Fig. S5A′). The WT cells and *pdgfrb* mutant cells took distinct positions in the UMAP of the cluster 3 and 6, reflecting their overall gene expression differences (Fig. S5B). The comparative scatterplot of average gene expression across WT and *pdgfrb*$^{-/-}$ conditions revealed that cluster 6 cells have more differential gene expression than cluster 3 cells (Fig. S5C). The mural cell markers were differentially expressed, with *kcne4* the most significantly different, in the WT cluster 6 cells compared with the *pdgfrb*$^{-/-}$ mutant cells (Fig. S5C, Table S4). These results indicate impaired smooth muscle cell differentiation in *pdgfrb* mutants even though low level expression of the smooth muscle and mural cell markers suggests that these cells still maintain mural cell identity. In contrast, the gene expression changes in the epicardial cluster (cluster 3) were less significant (Figs S3C and S5C). Among the epicardial markers, *tbx18* and *tcf21* showed prominent expression in the cluster 3 (epicardial cells) in both *pdgfrb* mutants and WT controls and much less expression in the cluster 6 (mural cells) (Fig. 3C′, Fig. S3C). These results suggested that in *pdgfrb* mutant heart, remaining epicardial cells and EPDCs (cluster 3) are less affected compared with differentiated mural cells (cluster 6), which decrease in number and change gene expression (Fig. S5A,A′,C).

Subclustering of the mural cells (cluster 6) revealed that subcluster 1 and 2, which have relatively higher *pdgfrb* expression and mural cell marker expression, are absent in *pdgfrb* mutants. Subcluster 0 cells have low *pdgfrb* but comparable *cxcl12b* expression with subcluster 1 and 2. Smooth muscle cell marker expression (*tagln*, *acta2*, *myh11a*) in subcluster 0 was also decreased in *pdgfrb* mutants (Fig. S6A,B, Table S5). A few cells in the epicardial cluster 3 also expressed some mural cell marker genes at a low level (*kcne4*, *tagln*, *notch3*) (Fig. 3C′, Fig. S3C). Further subclustering showed that subclusters 0, 1 and 3 express these mural cell markers along with epicardial markers and the fibroblast marker *pdgfra*. Subcluster 2 only expressed epicardial markers and likely are epicardial cells. Subcluster 4 expressed the mural cell marker *cd248a* and *kcne4*, along with the fibroblast marker *postnb* and *pdgfra* (Rajan et al., 2020) (Fig. S6C,D, Table S6). Thus, the epicardial *pdgfrb*-expressing cells are heterogeneous. Subclusters 0, 1, 3 and 4 are likely EPDCs showing genetic signatures of both mural cells and fibroblasts.

For functional analysis of *pdgfrb*-expressing cells, we performed gene ontology (GO) term analysis for differentially expressed genes in cluster 3 (epicardial cells) and cluster 6 (mural cells) cells compared with each other. The mural cells showed enrichment for GO terms related to development and morphogenesis, including ‘neuronal development’ and ‘blood vessel development/angiogenesis’. The epicardial cells showed GO term enrichment for ‘protein/peptide biosynthesis’ and ‘collagen and extracellular matrix synthesis’ (Fig. S7, Tables S7 and S8).

pdgfrb expression dynamically changes during heart regeneration

Our previous observation of *pdgfrb* upregulation and the presence of mural cells in the regenerating area of the zebrafish heart (Kim et al., 2010) prompted us to characterize *pdgfrb* expression patterns during regeneration. The apical regions of *Tg(pdgfrb:Citrine;fli1a:DsRed)* fish were injured and imaged at different days post-amputation (dpa). At 1 dpa, there were no obvious *pdgfrb*-expressing regions near the wound area except in mural cells around the pre-existing coronary vessels. Starting from 3 dpa, patchy *pdgfrb* expression was observed around the border of the amputated area (Fig. 4A). This expression gradually expanded significantly at 7 dpa and 10 dpa, plateaued at 14 dpa, and decreased at 30 dpa (Fig. 4A,A′, Fig. S8A). The mural cells associated with pre-existing coronary endothelial cells continued to express *pdgfrb* (Fig. S8A). This patchy *pdgfrb* expression was likely in epicardium or EPDCs because they were also positive for the epicardial marker *tcf21* (Fig. 4B). These *pdgfrb*$^{+}$ epicardial cells or EDPCs migrated and enveloped the regenerating area whereas the *pdgfrb*-expressing mural cells remained associated with the coronary endothelial cells migrating into the regenerating area.

We developed a novel fluidic device-based long-term explant culture for live imaging (Yip et al., 2020) to confirm the dynamic changes in *pdgfrb* expression patterns and potential interactions between *pdgfrb*$^{+}$ cells with other cell types. Hearts from transgenic zebrafish *Tg(pdgfrb:EGFP; fli1a:DsRed)* were injured and allowed to recover *in vivo* for 5-10 days, dissected out from the fish, then placed in the device for live imaging for 72-120 h. *pdgfrb:EGFP* expression at 5-6 dpa showed diffuse expression in the epicardium within most of the wound site and more localized expression in mural cells towards the edge and outside the wound site (Movie 1). As regeneration proceeded, *pdgfrb*$^{+}$ epicardial cells closed in to cover the entire wound area by 6 dpa. Following this, punctate, mural cell-like expression was observed within the regenerating region. The epicardial cells, or the diffuse expression observed within them, were highly dynamic within the wound area compared with the more stable behavior of existing mural cells (Movie 2). These mural cells migrated into the wound site alongside the individual endothelial cell to which they were attached (Movies 2 and 3). However, it was the dynamic epicardial expression or migration that preceded the endothelial cell migration into the

Development (2022) 149, dev199752. doi:10.1242/dev.199752

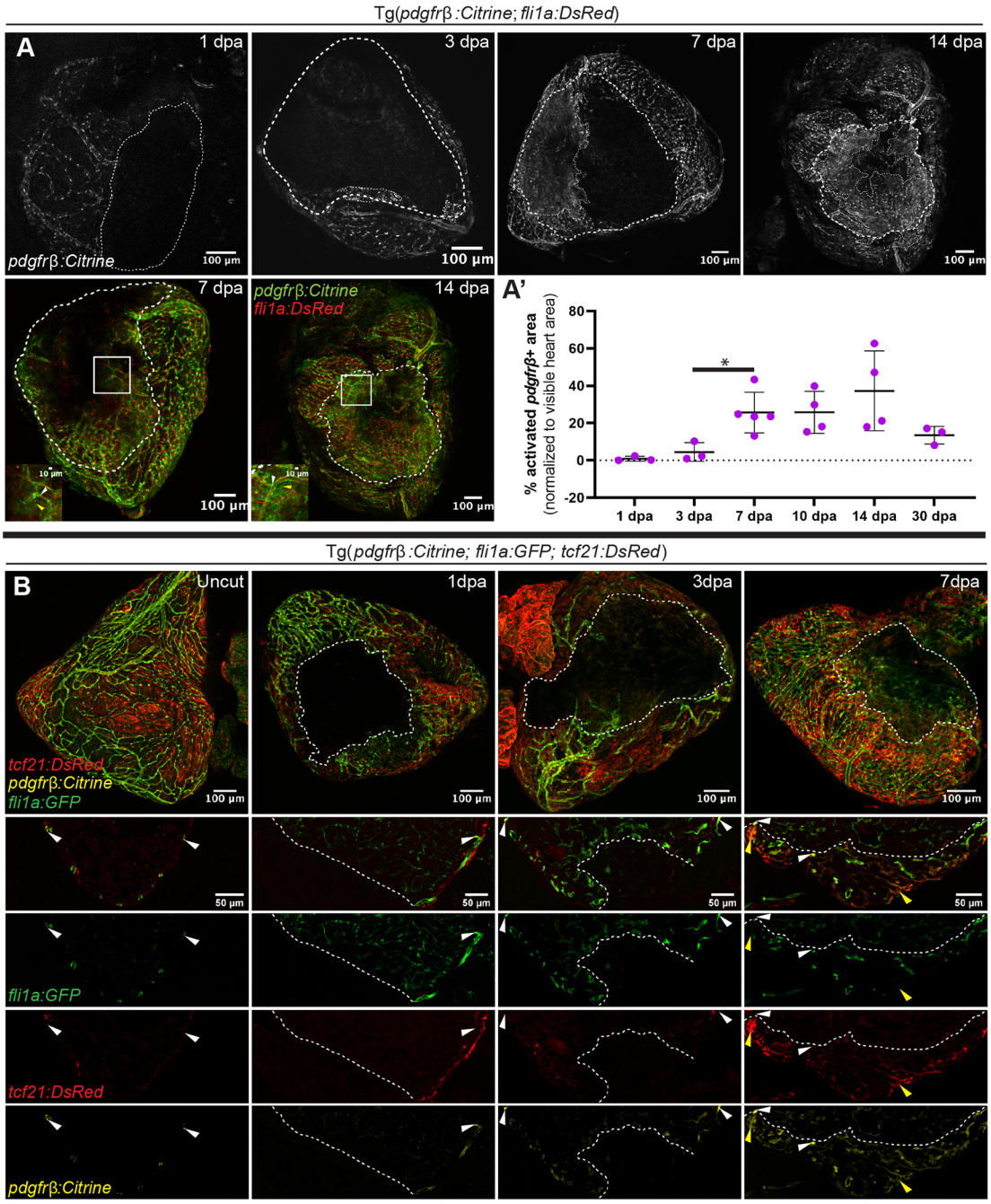

Fig. 4. Dynamic *pdgfrb* expression in the injured area during regeneration. (A,A′) *pdgfrb* expression early during heart regeneration. (A) *Tg(pdgfrb:Citrine; fli1a:DsRed)* fish hearts at 1, 3, 7 and 14 dpa. White dashed line indicates the injured area. White dotted line indicates the *pdgfrb*-expressing area. In the insets, white arrowheads indicate *pdgfrb* expression in mural cells and the yellow arrowheads non-mural cell *pdgfrb* expression. (A′) Quantification of the *pdgfrb*$^{+}$ area as a percentage of the imaged heart area. Error bars represent s.d. *P≤0.05 (one-way ANOVA). 1 day, 3 days, 30 days: n=3; 7 days: n=5; 10 days, 14 days: n=4. (B) *pdgfrb* expression in epicardium. *Tg(pdgfrb:Citrine; fli1a:EGFP; tcf21:DsRed)* fish hearts imaged as whole-mount preparations and as sections in uncut, 1, 3 and 7 dpa fish. White arrowheads indicate *pdgfrb* expression in mural cells; yellow arrowheads non-mural cell *pdgfrb* expression.

wound site. The pre-existing mural cell expression moved more slowly alongside the cell body of the endothelial cells, behind the filopodial extension (Movies 2 and 3). The imaging data described above suggest that two different *pdgfrb*$^{+}$ populations are present at the wound site during zebrafish heart regeneration: the pre-existing mural cells and a second epicardial cell-derived population. Furthermore, a subcomponent of the epicardium may be dynamically changing gene expression and transforming cell identity.

Heterogeneous epicardial and mural cells regulate heart regeneration

We hypothesized that *pdgfrb*$^{+}$ populations with essential roles in zebrafish heart regeneration might have more active gene expression. To characterize further the diverse *pdgfrb*$^{+}$ cell populations and determine their gene expression signatures, we performed FACS using WT adult *Tg(pdgfrb:EGFP; cxcl12b:Citrine)* zebrafish and FACS-sorted EGFP-positive cells from ventricles of uninjured and injured hearts at 7 dpa to perform

Development (2022) 149, dev199752. doi:10.1242/dev.199752

scRNAseq. The sorted EGFP$^+$ cells form 15 clusters based on their gene expression differences (Fig. S9A) and differentially expressed genes were identified (Fig. S9B, Table S9). The epicardial/EPDCs/mural cell cluster was identified based on marker gene expression (Table S9, Fig. S9C,D). Three-hundred and twelve cells from uninjured hearts and 199 cells from 7 dpa hearts (clusters 5, 6, 10 and 12 combined) were analyzed further (Fig. 5A,A′). We found that *pdgfrb* expression is mainly detected in clusters of epicardial cells/EPDCs/mural cells (clusters 5, 6, 10 and 12) (Fig. S9C,D). The heterogeneity of *tcf21:nucEGFP*$^+$ epicardial cells from uninjured hearts was previously reported (Cao et al., 2016). Therefore, we focused our gene signature analysis on the regenerating hearts.

By epicardial marker (*tcf21*, *tbx18*) and mural cell marker (*rgs5a*, *cd248a*, *kcne4*) (Cho et al., 2003; Venero Galanternik et al., 2017) gene expression, clusters 5, 6 and 10, were found to be epicardial/EPDC clusters, which have very few cells with mural cell marker expression, and cluster 12 was found to be the main mural cell cluster (Fig. S9D). Interestingly, when *pdgfrb* expression was checked across these clusters, the mural cell cluster (cluster 12) showed high *pdgfrb* expression but there was little to no difference in expression level between mural cells from uninjured and injured hearts. In all epicardial clusters, more cells from the injured hearts showed *pdgfrb* expression than uninjured heart cells (Fig. S9C). This is consistent with our observation that dynamic expression changes of *pdgfrb* in the injured hearts occur in the epicardial cells (Fig. 4). To characterize further overall gene expression changes in response to heart injury, differential gene expression analysis was performed combining all *pdgfrb*-expressing cluster cells (combining clusters 5, 6, 10 and 12 cells) for 7 dpa hearts compared with uninjured hearts (Fig. 5A′-C, Table S10).

Functional characterization of these *pdgfrb*-expressing cells was carried out by GO term analysis based on the differentially expressed genes in the injured hearts. After categorization of all enriched GO terms, it was found that functionalities related to extracellular matrix (ECM), collagen (16% of all GO terms), regeneration and development (12%), endopeptidase inhibitor activities (8%), supramolecular polymer changes in cytoskeleton (8%), extracellular space (6%), and response to oxygen level/hypoxia (6%) are enriched in the differentially expressed genes (Fig. 5D, Table S11). These functions are well-aligned with the requirements of a regenerating heart where ECM deposition occurs immediately after amputation. As the healing process progresses, cell migration and wound response/regeneration occur.

Fig. 5B shows the top 15 differentially expressed genes among the genes upregulated in the 7 dpa injured hearts based on the most significant adjusted *P*-values; some of them (*anxa2a*, *mdka*, *pdgfrl*, *si:ch211-198c19.3*) were validated by RT-PCR using FACS-sorted *pdgfrb:EGFP*$^+$ cells from 7 dpa hearts compared with uninjured hearts (Fig. S10B). The top 5 differentially expressed genes were: *zgc:152791*, *annexin A2a* (*anxa2a*), *fibronectin 1b* (*fn1b*), *midkine a* (*mdka*) and *periostin b* (*postnb*) (Fig. 5B). *anxa2a* has been recently shown to be required in zebrafish caudal fin regeneration (Quoseena et al., 2020). The ECM proteins Fibronectin 1b and Periostin b were previously shown to be upregulated/involved zebrafish heart regeneration (Rodius et al., 2014; Sanchez-Iranzo et al., 2018; Wang et al., 2013). *mdka*, encoding a growth factor, was previously shown to be induced after zebrafish heart injury, but its functions in heart regeneration after amputation have not been characterized (Lien et al., 2006).

Other upregulated genes at 7 dpa encode proteins including Hyaluronan and Proteoglycan link protein 1a (*hapln1a*), which is predicted to have hyaluronic acid-binding activity and has been shown to be involved in fin regeneration (Ouyang et al., 2017), epicardial EMT and heart regeneration (Missinato et al., 2015). Collagen type 1, alpha 1a (*col1a1a*) has also been shown to be involved in fin development and regeneration (Duran et al., 2015, 2011; Padhi et al., 2004). Thymosin beta 1 (*tmsb1*) and Chemokine ligand 8a (*cxcl8a*) are differentially expressed in clusters 5, 10 and 12, respectively (Table S9). Translation initiation factor (*eif4ebp3l*) and lipoprotein lipase (*lpl*) are two highly expressed genes in the uninjured hearts (Fig. S11A). Consistent with our previous findings (Kim et al., 2010), expression of epithelial-to-mesenchymal transition (EMT) genes (*snai1a*, *snai1b*, *snai2*, *twist1b*) were induced during heart regeneration (Fig. S11B). Overall, these data suggested that in response to zebrafish heart amputation the heterogeneous *pdgfrb*-expressing EPDCs and mural cells (clusters 5, 6, 10, 12) actively express genes with potential roles in heart regeneration (Fig. 5C). Further functional characterization by GO term enrichment analysis for individual *pdgfrb*$^+$ clusters indicated that the mural cell cluster (cluster 12) and epicardial/EPDC/fibroblast cluster (cluster 6) have the most potential roles in supporting tissue development and morphogenesis (17% of all GO term enrichment for each cluster). The mural cell cluster had the highest GO term enrichment for the circulatory system development (10% of all GO terms for cluster 12) followed by cluster 6 cells (7% of all GO terms for cluster 6). For clusters 5 and 10, 5% of each cluster's GO terms were related to circulatory system development. For cluster 10, which is the cluster expressing *postnb* in uninjured heart, 8% of the GO terms were related to immune system regulation (Fig. S12, Tables S12-S15).

pdgfrb is required for heart regeneration

We previously reported that fish treated with a Pdgfrβ inhibitor showed defects in revascularization during heart regeneration (Kim et al., 2010). Here, we utilized adult *pdgfrb* mutants to examine further the requirement of *pdgfrb* during zebrafish heart regeneration. We observed very few blood vessels in the regenerating area of *pdgfrb* mutant hearts at 21 and 34 dpa. These vessels were large, had significantly fewer branches, and were mostly devoid of *pdgfrb*$^+$ mural cells. In contrast, sibling control fish had dense networks of *pdgfrb*$^+$ mural cell-covered coronary vessels in the regenerating region (Fig. 6A). These data suggest that Pdgfrβ signaling plays an essential role during revascularization. The *pdgfrb* mutants failed to regenerate after ventricular resection and maintained a fibrotic scar (Fig. 6B), confirming that Pdgfrβ signaling is essential for heart regeneration. *mdka* was found as one of the top differentially expressed genes (Fig. 5B) and showed increased expression in 7 dpa hearts. We confirmed the upregulation of *mdka* in EDPCs by qRT-PCR using FACS-sorted *pdgfrb:EGFP*$^+$ cells and by *in situ* hybridization. qRT-PCR using 7 dpa whole heart ventricles further validated the upregulation of *mdka* whereas *mdkb* expression did not increase (Fig. S13A-C). Midkine (Mdk) has been shown to play important roles in tissue regeneration in many different organs in multiple species (Ang et al., 2020; Ikutomo et al., 2014; Nagashima et al., 2020; Tsai et al., 2020). However, in contrast to *pdgfrb* mutant hearts, *mdka* mutants did not show significant defects in heart regeneration (Fig. S13D) and collagen deposition (Fig. S13E,E′), despite its strong expression.

DISCUSSION

The cell compositions, functions and origins of the mural cells in the hearts remain incompletely understood. Focusing on *pdgfrb*$^+$ cells, we determined the heterogeneity of these cardiac mural cells and EPDCs in zebrafish heart during development and regeneration and

Development (2022) 149, dev199752. doi:10.1242/dev.199752

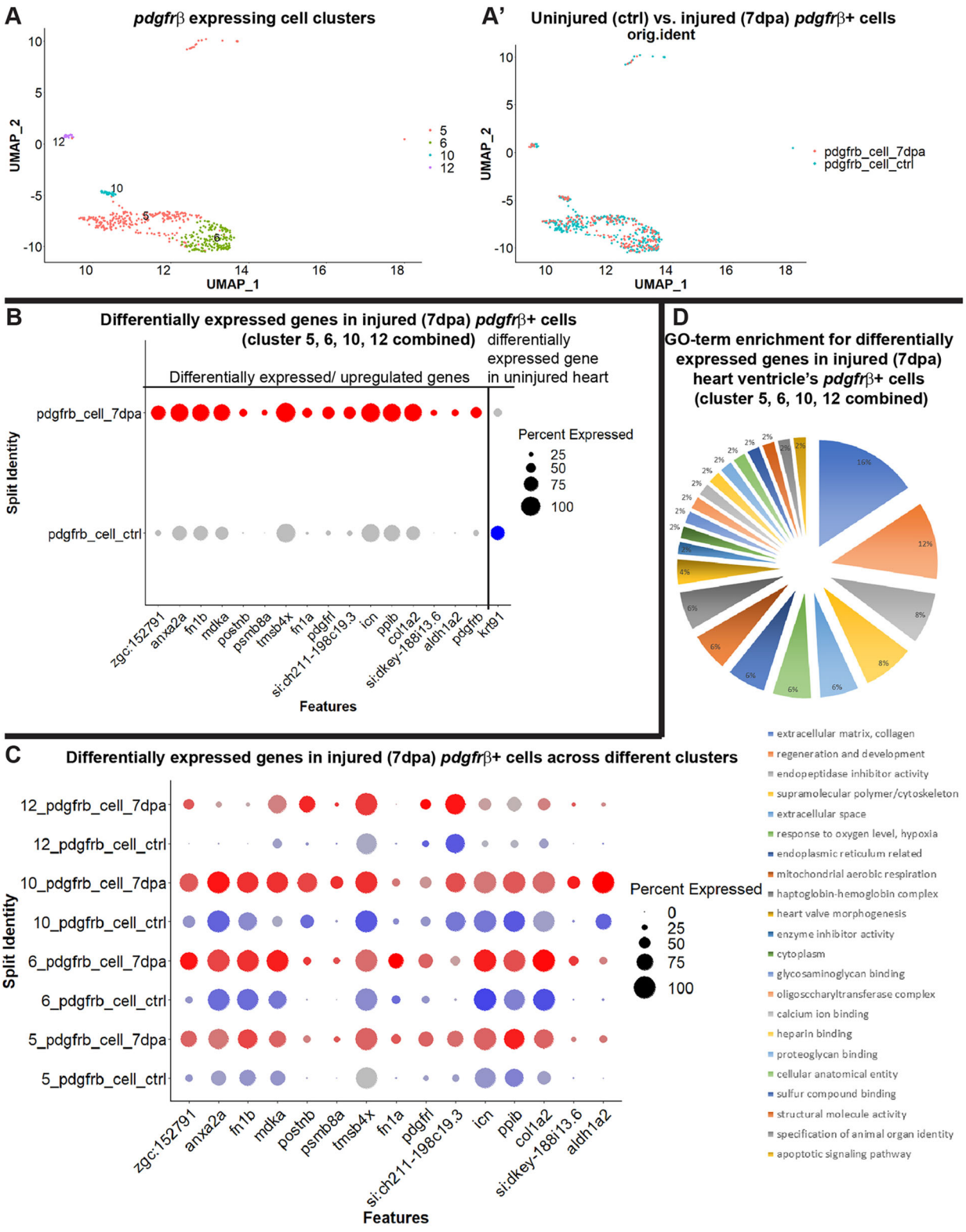

Fig. 5. Characterization of the *pdgfrb*$^{+}$ cells in regenerating hearts after amputation. (A,A′) The epicardial/EPDC and mural cell clusters (5, 6, 10 and 12) of FACS-sorted *pdgfrb:EGFP*$^{+}$ from uninjured and injured (7 dpa) fish hearts. (A) UMAP plot of integrated uninjured and 7 dpa epicardial/EPDC and mural cells. (A′) UMAP plot of cells from uninjured (blue) and 7 dpa (red) hearts. (B) Dot plot of the differentially expressed genes in FACS-sorted *pdgfrb:EGFP*-expressing cells analyzed by combining clusters 5, 6, 10 and 12. Blue dot, represents uninjured hearts. Red dots represent 7 dpa hearts. Expression level across cells within the cluster is shown by intensity of the color and the percentage of the cells expressing the marker gene is shown by the size of the dot (0-100%). Differentially expressed genes were determined with minimum percent expression cut-off=0.1 and minimum average log fold change=0.25, adjusted $P \leq 0.001$. (C) Dot plot of the differentially expressed genes in FACS-sorted *pdgfrb:EGFP*-expressing cells in clusters 5, 6, 10 and 12. (D) Categorizations and relative enrichments of GO terms derived from the differentially expressed genes in the combined clusters 5, 6, 10 and 12. Genes are selected with adjusted *P*-value≤0.1 and enriched GO terms were selected with Holm–Bonferroni correction $P \leq 0.05$.

Development (2022) 149, dev199752. doi:10.1242/dev.199752

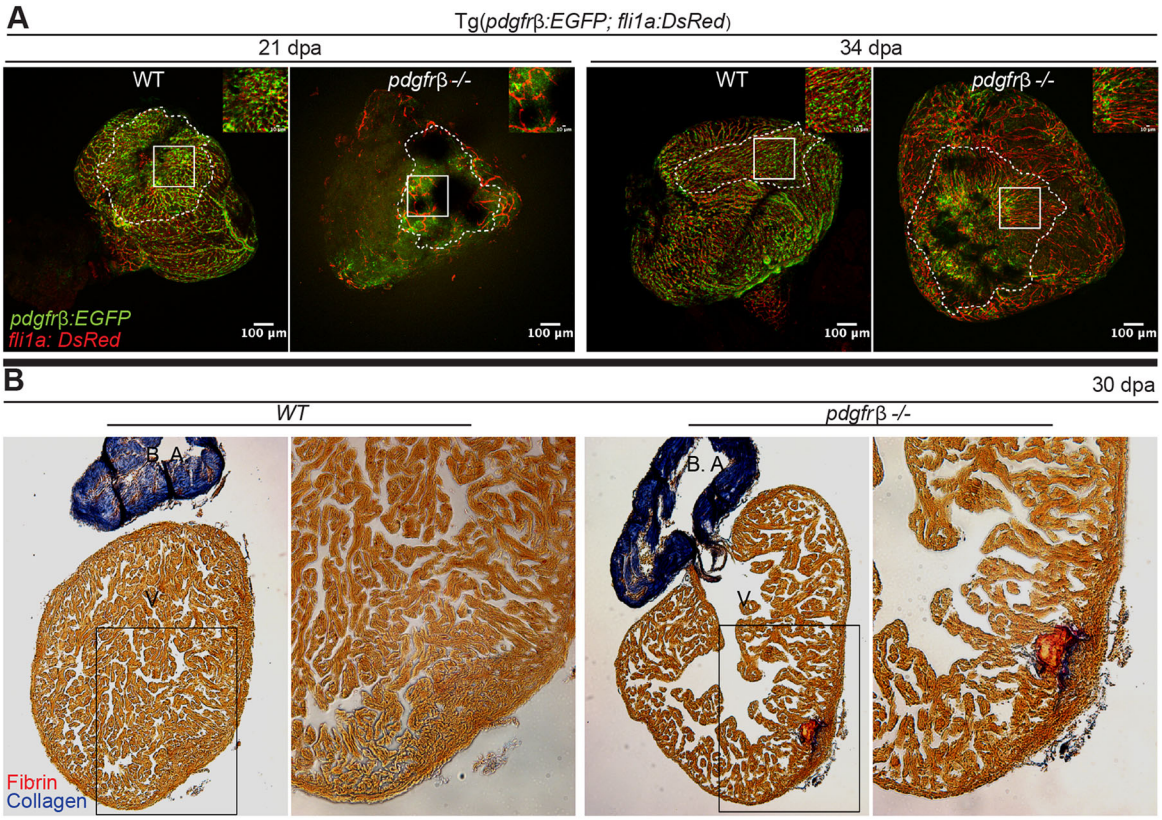

Fig. 6. *pdgfrb* mutant hearts fail to regenerate and form a fibrotic scar. (A) *pdgfrb* mutant fish cannot revascularize the regenerating area of the amputated heart. *pdgfrb*$^{+/+}$ fish have dense network of coronary vasculature (*pdgfrb:EGFP*, green; *fli1a:DsRed*, red) in the regenerating area at 21 and 34 dpa whereas the *pdgfrb* mutants have very few coronary vessels with network formation. Unlike WT, the coronary vessels in the *pdgfrb* mutant lack the *pdgfrb*$^{+}$ mural cell coverage in the regenerating area (*n*=4). (B) Acid Fuchsin Orange G staining of heart sections of WT and *pdgfrb* mutants at 30 dpa. *n*=7. Images to the right show enlarged views of the boxed areas to the left. B.A. bulbus arteriosus; V, ventricle.

investigated how Pdgfrβ signaling affects these different cell populations. We found that, during heart development, *pdgfrb* and *cxcl12b* double-positive (*pdgfrb*$^{+}$;*cxcl12b*$^{+}$) cells line coronary arteries whereas mural cells expressing only *pdgfrb* surround non-arterial vessels. Furthermore, *pdgfrb*$^{+}$ EPDCs are less affected than mural cells in *pdgfrb*$^{+}$ mutant hearts. In adult regenerating hearts, *pdgfrb*$^{+}$ cells were identified in pre-existing mural cells and EPDCs. The use of scRNAseq and confocal and live imaging allowed us to delineate unique gene expression signatures in different populations, revealing their different functions.

Although very few *pdgfrb*$^{+}$;*cxcl12b*$^{+}$ double-positive cells were captured in our scRNAseq analysis, smooth muscle gene expression in these double-positive cells suggests that they are more differentiated than the *pdgfrb*$^{+}$ only cells. Interestingly, the association of these *pdgfrb*$^{+}$;*cxcl12b*$^{+}$ mural cells with coronary arteries does not depend on Pdgfrβ signaling and all non-arterial vessels lose *pdgfrb*$^{+}$ mural cells in *pdgfrb* mutants. Recent scRNAseq data of mouse brain revealed two subclasses of mural cells; pericytes are in a continuum with venous smooth muscle cells, which are distinct from arteriole or arterial smooth muscle cells (Vanlandewijck et al., 2018). It is possible that *pdgfrb*$^{+}$;*cxcl12b*$^{+}$ mural cells are similar to arteriole or arterial smooth muscle cells, which are different from the *pdgfrb*$^{+}$ only cells surrounding the wide large vessels that are likely the coronary veins. In mice, smooth muscle cells along the coronary arteries are derived from *Pdgfrb*$^{+}$ pericyte progenitors after the blood flow starts but the smooth muscle cells around the coronary arteries fail to form in Pdgfrβ knockout mice (Volz et al., 2015). However, these *pdgfrb*$^{+}$;*cxcl12b*$^{+}$ double-positive cells remained associated with coronary arteries in *pdgfrb* mutant fish, suggesting that a previously unknown mechanism exists to maintain the mural cell association with coronary arteries. One likely mechanism is that Cxcl12-Cxcr4 signaling (Stratman et al., 2020) might activate an alternative signaling pathway in the arterial mural cells that acts in parallel with PDGF signaling for mural cell recruitment. The scRNAseq identified several signaling pathways that could mediate this Pdgfrβ-independent mural cell association with coronary endothelial cells and this will be pursued in future investigation. Furthermore, our scRNAseq analyses also revealed new mural cell markers, *kcne4* and *ndufa4l2a*, that are affected in *pdgfrb* mutants, consistent with recently reported results in zebrafish embryos (Shih et al., 2021).

Pdgfrβ signaling and *pdgfrb*$^{+}$ cells have been implicated in the development and regeneration of different tissues and organs. Consistent with our finding, intra-myocardial delivery of PDGF-BB provides myocardial protection and improves ventricular functions (Hsieh et al., 2006a,b). Nonetheless, our current findings cannot distinguish between a phenotype in EPDCs versus a developmental phenotype in coronary vessels or revascularization that resulted in the impaired heart regeneration in *pdgfrb* mutants. A temporospatial-specific knockdown of *pdgfrb* during heart regeneration will be performed in the future to elucidate this mechanism further. Recently, it was demonstrated that ECM derived from *pdgfrb*$^{+}$ myoseptal and perivascular cells prevents scarring and promotes axon regeneration of zebrafish spinal cord in a Pdgfrβ signaling-dependent manner (Tsata et al., 2021). Consistent with this finding, our scRNAseq analyses identified

Development (2022) 149, dev199752. doi:10.1242/dev.199752

significant changes (16% of all GO term enrichment) in genes encoding ECM components. How Pdgfrβ signaling regulates the ECM in the regenerating heart and shapes the regenerative environment will be of interest for future studies.

Taking a candidate approach to examine further the differentially expressed genes identified from our scRNAseq, we decided to first assess the roles of *mdka*, which was also discovered by microarray gene expression profiling previously (Lien et al., 2006). *mdka* has been shown to play an important role in neural regeneration in the retina by regulating cell cycle progression of Müller glia (Nagashima et al., 2020), epimorphic regeneration (Ang et al., 2020) and regeneration after skeletal muscle injury (Ikutomo et al., 2014). Furthermore, it was recently reported that axolotl Midkine (Mdk) could regulate wound epidermis development and inflammation during the initiation of limb regeneration (Tsai et al., 2020). *mdka* is highly expressed in epicardium and EPDCs after amputation and this led us to examine its role during heart regeneration. We did not observe any significant defects in heart regeneration and increased fibrotic scarring remained at the injury site at 34 dpa compared with controls. However, it was reported that loss of *mdka* after cryoinjury decreased proliferation of endothelial cells and retention of a collagen scar (Grivas et al., 2021). We cannot exclude the possibility that different *mdka* mutant alleles and injury models might reveal regeneration defects. Examining the phenotypes of different *mdka* mutant alleles in cryoinjury versus amputation injury models is of interest for future investigation; however, is beyond the scope the current study. Nonetheless, our scRNAseq data provide new candidate genes that may have a role in coronary vessel development and heart regeneration.

MATERIALS AND METHODS

Fish lines

The following zebrafish lines were raised and maintained at Children's Hospital Los Angeles (CHLA) under standard conditions of care and with CHLA IACUC oversight. IACUC approved all experimental procedures used in this study. Both males and females were utilized in this study. The age and length of the fish are specified in the results. The fish lines used in this study were: *Tg(fli1a.ep:DsRedEX)*^{um13} (also known as *fli1a:DsRed*; Covassin et al., 2007), *Tg(fli1a:EGFP)* (Lawson and Weinstein, 2002), *TgBAC(pdgfrb:EGFP)* (Ando et al., 2016), *TgBAC(pdgfrb:Citrine)* (Vanhollebeke et al., 2015), *pdgfrb*^{um148} (Kok et al., 2015), *Mdka*^{mi5001}(Nagashima et al., 2020), *Tg(cxcl12b:Citrine)* (Bussmann et al., 2011), *TgBAC(tcf21:Cre-ERT2)*^{pd42} (Kikuchi et al., 2011), *Tg(-3.5ubi:loxP-EGFP-loxP-mCherry)* (Mosimann et al., 2011) and *Tp1bglb:Venus-PEST* (Ninov et al., 2012).

Lineage tracing *tcf21:CreERT2* was performed as described by Harrison et al. (2015) with *pdgfrb:Citrine* as the mural cell marker. *Tg(pdgfrb:Citrine; tcf21:CreERT2; ubi:loxp-EGFP-loxp-mCherry)* fish were generated and the embryonic epicardial cells were labeled by mCherry by activating *tcf21:CreERT2* by administering 4-hydroxytamoxiphen (4-OHT) during the first 5 days of embryonic development. 4-OHT (13 µg/ml) was added to E3 medium and the medium was changed daily. After treatment, the fish were raised into adulthood. The adult hearts carried all the progenies derived from the embryonic-labeled epicardium. *pdgfrb:Citrine* was used to identify the mural cells. The percentage of mCherry-labeled Citrine-positive cells was quantified.

Angiography dye injection and amputation

Dextran Cascade Blue dye was injected through the retro-orbital sinus as described (Harrison et al., 2015). Briefly, injection was performed 2.5-3.0 h before heart extraction. Zebrafish were anesthetized in a tricaine solution and placed horizontally on a sponge so that the right eye was facing up. A Hamilton syringe loaded with 4 pl Dextran Cascade Blue was inserted at 30° to the plane of the sponge, about 2 mm deep at the 7 o'clock position of the right eye socket (Pugach et al., 2009). The amputation experiments were performed as described (Poss et al., 2002).

Confocal imaging

Hearts were immobilized in 1% low melting point agarose in PBS. The heart was oriented with the ventricle at the center of the image, the bulbus arteriosus at the top, and the atrium on the left. *z*-stack images were collected using a Zeiss 710 confocal microscope. *z*-stack images were then converted to a maximum intensity projection before further processing/quantification. ImageJ/Fiji software was used for quantification.

Live imaging

Hearts from transgenic zebrafish [*Tg(pdgfrb:EGFP; fli1a:DsRed)*] were amputated and allowed to recover *in vivo* for 5-10 days, after which hearts were removed into imaging media [L15 (300 ml), 10% fetal calf serum/fetal bovine serum, 100 µg/ml Primocin, 1.25 mM $CaCl_2$, 800 mg/l glucose, Pen/Step]. Hearts were cleaned of any external blood or attached tissue debris. The imaging microfluidic device was prepared as described (Yip et al., 2020) and four hearts were then placed into the imaging wells under Ringer's solution. The device was sealed and mounted onto a Zeiss cell observer system equipped with a Hamamatsu ORCA-flash4.0LT and Colibri 7 LED light source for live imaging. The imaging device was maintained at a temperature of 28.5°C with a PeCon atmospheric control stage and cover. Imaging media was perfused through the imaging wells at a rate of 0.5 ml/h and imaging was carried out for 72-120 h. Acquisitions were carried out to capture a *z*-stack of 35-50 images 6 µm apart every 30 min. Collected images were cropped (in *z*-plane and time) and deconvolved (using AutoQuant). ImageJ/Fiji was used to produce the final moves with the aid of a Gaussian-based focusing macro and a z sub-selection macro (available on request).

Quantification

Mural cell association

Mural cell association with the coronary vessels was quantified as the mural cell number per unit vessel length. Using ImageJ software, freehand lines were drawn along the length of randomly selected vessels of certain size (e.g. Fig. 2B′) or from certain regions of the heart ventricles (e.g. Fig. 1B). The length (by pixel numbers) of the freehand line was measured by ImageJ and *pdgfrb*$^{+}$ cells along the line were counted manually. Then, the *pdgfrb*$^{+}$ cell numbers were divided by the freehand line's length to get the measurement of the mural cell number per unit vessel length. Paired *t*-test was used to quantify the significance of the value differences between different samples.

Ventricle coverage by coronary vessels

Using ImageJ freehand selection tools, areas covered by coronary vessels following the tips of the vessels were selected in heart ventricles. Respective areas were measured and the areas following the coronary vessels were divided by whole ventricle area and corresponding percentages were quantified (Fig. 2A′). One-way ANOVA was used to quantify the significance of the value differences between *pdgfrb*$^{+/+}$, *pdgfrb*$^{+/-}$ and *pdgfrb*$^{-/-}$ hearts.

pdgfrb expression during regeneration

pdgfrb expression was quantified by measuring the area of the *pdgfrb*-expressing region as a percentage of the area of the whole apical view of the ventricle (Fig. 4A′). The area of the *pdgfrb*-expressing region (marked by the white small-dotted line in Fig. 4A) was quantified using the freehand selection tool of ImageJ software. One-way ANOVA was used to quantify the significance of the measurement difference between 3 dpa and 7 dpa.

Heart tissue dissociation into single-cell suspension

The heart ventricle was immersed in the modified Tyrode's solution (Tessadori et al., 2012) on ice. After washing blood from the tissue, the ventricle was torn open and into small pieces by forceps and transferred into Ca^{2+}-free modified Tyrode's solution (Tessadori et al., 2012) at 30°C. The tissue was then washed twice with ice-cold Ca^{2+}-free modified Tyrode's

Development (2022) 149, dev199752. doi:10.1242/dev.199752

solution. The tissue was then treated with the digestion mix (500 µl per five hearts) containing Liberase (500 CDU); Elastase (3.1 U) and DNaseI (32 U) at 33-35°C for ∼15 min with continuous stirring. The digestion was stopped by adding ice-cold Ca^{2+}-free modified Tyrode's solution containing 10% fetal bovine serum and DNaseI (32 U). The solution was then filtered through a 40-µm sieve and the cells were pelleted by centrifuging at 500 ***g*** for 5 min at 4°C. The cells were washed with ice-cold Ca^{2+}-free modified Tyrode's solution containing 30% fetal bovine serum. The cells were then precipitated again and redissolved in an appropriate volume of ice-cold Ca^{2+}-free modified Tyrode's solution containing 30% fetal bovine serum to maintain a suitable cell density for single-cell cDNA library preparation or qRT-PCR.

FACS sorting of *pdgfrb:EGFP* cells

pdgfrb:EGFP cells were FACS-sorted from *Tg(pdgfrb:EGFP*; *cxcl12b:Citrine)* 6-month-old WT and *pdgfrb*$^{-/-}$ fish. *pdgfrb:EGFP* cells were FACS-sorted from approximately ten *Tg(pdgfrb:EGFP*; *cxcl12b:Citrine)* 18-month-old uninjured or injured (7 dpa) fish. Heart ventricles were dissociated into single-cell suspension following the abovementioned method for each sample. *pdgfrb:EGFP* cells were FACS-sorted using a BD FACSAria cell sorter. The live cells were sorted by filtering out dead cells with DAPI staining. EGFP only, DsRed only transgenic samples were used as a positive control, and WT fish without any transgenic reporter were used as the negative control. During sorting, the FACS gates were set to maximize inclusion of all GFP-positive cells (low to high EGFP signals) to isolate all possible EGFP-expressing cell populations. This wide gate set-up led to the inclusion of other cell types (e.g. cardiomyocytes) that do not express *pdgfrb:EGFP*, likely due to background fluorescence. After sorting, the cells were collected into Ca^{2+}-free modified Tyrode's solution containing 30% fetal bovine serum and kept on ice. This solution was then centrifuged at 500 ***g*** for 5 min at 4°C to concentrate the sample for downstream procedures (e.g. single-cell RNA sequencing, qRT-PCR). For qRT-PCR, the FACS gates for sorting GFP^{+} cells were divided to isolate cells expressing GFP at a high level separately from those expressing GFP at a moderate level based on our confocal imaging and scRNAseq observations that coronary arterial mural cells are GFP^{high} cells whereas GFP^{low} cells include mostly epicardial cells.

scRNAseq

For the generation of single-cell gel beads in emulsion, cells were loaded on a Chromium single cell instrument (10X Genomics) following the manufacturer's protocol. In brief, a single-cell suspension of cells in 0.4% bovine serum albumin in PBS were added to each channel on the 10X chip. Cells were partitioned with gel beads into emulsion in the Chromium instrument in which cell lysis and barcoded reverse transcription of RNA occurred following amplification. scRNAseq libraries were prepared using the Chromium single cell 3′ library and gel bead kit v3 (10X Genomics). Sequencing was performed on HiSeq platform (Illumina), and the digital expression matrix was generated using the Cell Ranger pipeline (10X Genomics). In total, 1833 (99,466 mean reads per cells) and 1504 (67,463 mean reads per cell) *pdgfrb:EGFP* cells were sequenced for control and *pdgfrb* mutant hearts, respectively. After removing low-quality cells, we analyzed 955 and 1126 cells from control and *pdgfrb* mutant hearts, respectively. From a combined dataset of control and *pdgfrb* mutant hearts (955+1126 cells), 274 *pdgfrb* only and 126 *pdgfrb; cxcl12b* cells were identified and analyzed from 5826 cells from uninjured hearts and 3127 cells from regenerating WT adult hearts with an average of 29,327 and 66,193 reads per cell, respectively. After removing low-quality cells, finally we analyzed 1631 cells from uninjured hearts and 1097 cells from 7 dpa hearts. From combined dataset of uninjured and injured hearts (1631+1097 cells), 511 *pdgfrb* cells or epicardial/EPDC/mural cells were identified and analyzed using the Seurat R package.

scRNAseq data analysis

To identify different cell types and find signature genes for each cell type, the R package Seurat (version 3.2.3) was used to analyze the digital expression matrix. Cells with <100 and >2500 unique feature count and >25% mitochondrial expression were removed from further analysis. The Seurat function NormalizeData was used to normalize the raw counts. Variable genes were identified using the FindVariableGenes function. The Seurat ScaleData function was used to scale and center expression values in the dataset for dimensional reduction. Principal component analysis, t-distributed stochastic neighbor embedding and UMAP were used to reduce the dimensions of the data, and the first two dimensions were used in plots. The FindClusters function was later used to cluster the cells. The FindAllMarkers function was used to determine the marker genes for each cluster, which were then used to define cell types. Also, known cell type marker expression was determined across different clusters to assign the cell type to a cluster. We integrated the WT and *pdgfrb*$^{-/-}$ dataset together. Also, we integrated uninjured and injured (7 dpa) datasets using pairwise anchors by Seurat. After clustering cells based on the differentially expressed genes, cell types were identified by marker gene expression. For GO term analysis, differentially expressed genes in a cluster were selected with adjusted *P*-value<0.1. The selected genes were then put in a list form at http://www.zebrafishmine.org for GO term analysis. Enriched GO terms were generally selected after running Holm–Bonferroni or Benjamini–Hochberg corrections with *P*-value<0.05. All the GO terms were then categorized based on common criteria (e.g. similar expression location, functional similarities, structural similarities, etc.) and their relative percentages were presented as a pie chart. Different plots (e.g. violin plots, dot plots, feature plots) were made following available default Seurat codes. The Subset function was used for isolating and comparing different cell populations either from different clusters (Fig. 3C, Table S2, cluster 6 versus cluster 3 cells), or expressing/not expressing certain genes (Fig. 3D, Table S3, *cxcl12b*$^{+}$ versus *cxcl12b*$^{-}$ cells from cluster 6) or from WT versus *pdgfrb* mutant (from cluster 6, Table S4) or *pdgfrb*-expressing cells from injured (7 dpa) versus uninjured hearts (combining clusters 5, 6, 10 and 12; Fig. 5B, Table S10). Separate Seurat objects were formed with the isolated cells and merged together to identify differentially expressed genes in the desired group of cells (Fig. 3D, Table S3, *cxcl12b*$^{+}$ versus *cxcl12b*$^{-}$ cells). For *cxcl12b*$^{+}$ cells from cluster 6, *cxcl12b* expression level >0 was used to subset *cxcl12b*$^{+}$ cells and *cxcl12b*≤0 was used to subset *cxcl12b*$^{-}$ cells (Fig. 3D).

qRT-PCR

To validate candidate genes found in the mural cell cluster by scRNAseq, qRT-PCR was performed with cDNAs of GFP^{high} cells compared with GFP^{low} cells (Fig. S4). For validating upregulated genes in the injured (7 dpa) heart *pdgfrb*-expressing cells (Fig. 5B), cDNAs from GFP^{high} cells and GFP^{low} cells were mixed in a 1:1 ratio for each sample for qRT-PCR (Fig. S10). FACS-sorted *pdgfrb:EGFP* cells or *fli1a:DsRed* cells or whole-ventricle samples were collected in Trizol for RNA extraction by the Trizol-chloroform method. The RNAs were precipitated overnight at −20°C in isopropanol and washed with 70% alcohol and dissolved in DEPC-treated water. cDNAs were made from the RNA using the SuperScript® III First-Strand Synthesis System. qRT-PCR was performed using Applied Biosystems® SYBR® Green PCR Master Mix. Gene expression fold changes were normalized to the housekeeping gene *rpl13*. The mean cycle threshold (Ct) values of each sample triplicate were calculated and $2^{-\Delta\Delta Ct}$ values were calculated for each sample to determine expression fold changes. See Table S16 for qRT-PCR primers.

Acknowledgements

We thank Drs Koji Ando and Christer Betsholtz for discussions and communications prior to the submission; Dr Didier Stainier for the *pdgfrb:Citrine* line; Drs Koji Ando and Hiro Nakajima for the *pdgfrb:EGFP* line; and Dr Ken Poss for the *tcf21:dsRed* line. We also thank the TSRI Cellular Imaging, FACS and Single-Cells, Sequencing and CyTOF (SC2) cores.

Competing interests

The authors declare no competing or financial interests.

Author contributions

Conceptualization: S.K., H.B., J.F., Y.H., K.M.W., M.M.R.H., C.-L.L.; Methodology: S.K., H.B.; Software: S.K., F.M., M.P.; Validation: S.K., H.B., J.F., Y.H.; Formal analysis: S.K., H.B., J.F., Y.H., F.M., T.Y., A.A., M.M.R.H.; Resources: F.K., J.K.Y., M.L.M., M.P., M.N., P.F.H., N.M., N.D.L.; Data curation: S.K., H.B., J.F., Y.H., T.Y.,

A.A., K.M.W., J.K.Y., M.M.R.H.; Writing - original draft: S.K., H.B., J.F., K.M.W., M.M.R.H., C.-L.L.; Writing - review & editing: S.K., F.K., P.F.H., N.D.L., M.M.R.H., C.-L.L.; Supervision: M.L.M., M.P., P.F.H., M.M.R.H., C.-L.L.; Project administration: C.-L.L.; Funding acquisition: C.-L.L.

Funding

This research was funded by the Saban Research Institute Children's Hospital Los Angeles Intramural 2nd NIH R01 Pilot Grant and Team Awards (C.-L.L.), the National Institutes of Health (R01HL130172 to C.-L.L., R01EY007060 to P.F.H., P30EY007003 to P.F.H.), and Research to Prevent Blindness (P.F.H.). Deposited in PMC for release after 12 months.

Data availability

Raw data files for *pdgfrb:EGFP* FACS-sorted cells in *pdgfrb* mutants, WT (scRNAseq data of Fig. 3 and Figs S3, S5, S6, S7) and WT uninjured and 7 dpa (scRNAseq data of Fig. 5 and Figs S9, S11, S12) fish are available at Gene Expression Ominibus under accession number GSE188511.

Peer review history

The peer review history is available online at https://journals.biologists.com/dev/article-lookup/doi/10.1242/dev.199752.

References

Ando, K., Fukuhara, S., Izumi, N., Nakajima, H., Fukui, H., Kelsh, R. N. and Mochizuki, N. (2016). Clarification of mural cell coverage of vascular endothelial cells by live imaging of zebrafish. *Development* **143**, 1328-1339. doi:10.1242/dev.132654

Ando, K., Shih, Y.-H., Ebarasi, L., Grosse, A., Portman, D., Chiba, A., Mattonet, K., Gerri, C., Stainier, D. Y. R., Mochizuki, N. et al. (2021). Conserved and context-dependent roles for pdgfrb signaling during zebrafish vascular mural cell development. *Dev. Biol.* **479**, 11-22. doi:10.1016/j.ydbio.2021.06.010

Ang, N. B., Saera-Vila, A., Walsh, C., Hitchcock, P. F., Kahana, A., Thummel, R. and Nagashima, M. (2020). Midkine-a functions as a universal regulator of proliferation during epimorphic regeneration in adult zebrafish. *PLoS ONE* **15**, e0232308. doi:10.1371/journal.pone.0232308

Armulik, A., Abramsson, A. and Betsholtz, C. (2005). Endothelial/pericyte interactions. *Circ. Res.* **97**, 512-523. doi:10.1161/01.RES.0000182903.16652.d7

Armulik, A., Genove, G. and Betsholtz, C. (2011). Pericytes: developmental, physiological, and pathological perspectives, problems, and promises. *Dev. Cell* **21**, 193-215. doi:10.1016/j.devcel.2011.07.001

Bussmann, J., Wolfe, S. A. and Siekmann, A. F. (2011). Arterial-venous network formation during brain vascularization involves hemodynamic regulation of chemokine signaling. *Development* **138**, 1717-1726. doi:10.1242/dev.059881

Cai, C.-L., Martin, J. C., Sun, Y., Cui, L., Wang, L., Ouyang, K., Yang, L., Bu, L., Liang, X., Zhang, X. et al. (2008). A myocardial lineage derives from Tbx18 epicardial cells. *Nature* **454**, 104-108. doi:10.1038/nature06969

Cao, J., Navis, A., Cox, B. D., Dickson, A. L., Gemberling, M., Karra, R., Bagnat, M. and Poss, K. D. (2016). Single epicardial cell transcriptome sequencing identifies Caveolin 1 as an essential factor in zebrafish heart regeneration. *Development* **143**, 232-243. doi:10.1242/dev.130534

Chen, Q., Zhang, H., Liu, Y., Adams, S., Eilken, H., Stehling, M., Corada, M., Dejana, E., Zhou, B. and Adams, R. H. (2016). Endothelial cells are progenitors of cardiac pericytes and vascular smooth muscle cells. *Nat. Commun.* **7**, 12422. doi:10.1038/ncomms12422

Cho, H., Kozasa, T., Bondjers, C., Betsholtz, C. and Kehrl, J. H. (2003). Pericyte-specific expression of Rgs5: implications for PDGF and EDG receptor signaling during vascular maturation. *FASEB J.* **17**, 440-442. doi:10.1096/fj.02-0340fje

Covassin, L. D., Siekmann, A. F., Kacergis, M. C., Laver, E., Moore, J. C., Villefranc, J. A., Weinstein, B. M. and Lawson, N. D. (2009). A genetic screen for vascular mutants in zebrafish reveals dynamic roles for Vegf/Plcg1 signaling during artery development. *Dev. Biol.* **329**, 212-226. doi:10.1016/j.ydbio.2009.02.031

Duran, I., Mari-Beffa, M., Santamaria, J. A., Becerra, J. and Santos-Ruiz, L. (2011). Actinotrichia collagens and their role in fin formation. *Dev. Biol.* **354**, 160-172. doi:10.1016/j.ydbio.2011.03.014

Duran, I., Csukasi, F., Taylor, S. P., Krakow, D., Becerra, J., Bombarely, A. and Mari-Beffa, M. (2015). Collagen duplicate genes of bone and cartilage participate during regeneration of zebrafish fin skeleton. *Gene Expr. Patterns* **19**, 60-69. doi:10.1016/j.gep.2015.07.004

Grivas, D., Gonzalez-Rajal, A. and De La Pompa, J. L. (2021). Midkine-a regulates the formation of a fibrotic scar during zebrafish heart regeneration. *Front. Cell Dev. Biol.* **9**, 669439. doi:10.3389/fcell.2021.669439

Harrison, M. R. M., Bussmann, J., Huang, Y., Zhao, L., Osorio, A., Burns, C. G., Burns, C. E., Sucov, H. M., Siekmann, A. F. and Lien, C.-L. (2015). Chemokine-guided angiogenesis directs coronary vasculature formation in zebrafish. *Dev. Cell* **33**, 442-454. doi:10.1016/j.devcel.2015.04.001

He, L., Vanlandewijck, M., Raschperger, E., Andaloussi Mäe, M., Jung, B., Lebouvier, T., Ando, K., Hofmann, J., Keller, A. and Betsholtz, C. (2016). Analysis of the brain mural cell transcriptome. *Sci. Rep.* **6**, 35108. doi:10.1038/srep35108

Hellstrom, M., Kalen, M., Lindahl, P., Abramsson, A. and Betsholtz, C. (1999). Role of PDGF-B and PDGFR-beta in recruitment of vascular smooth muscle cells and pericytes during embryonic blood vessel formation in the mouse. *Development* **126**, 3047-3055. doi:10.1242/dev.126.14.3047

Hsieh, P. C., Davis, M. E., Gannon, J., Macgillivray, C. and Lee, R. T. (2006a). Controlled delivery of PDGF-BB for myocardial protection using injectable self-assembling peptide nanofibers. *J. Clin. Invest.* **116**, 237-248. doi:10.1172/JCI25878

Hsieh, P. C. H., Macgillivray, C., Gannon, J., Cruz, F. U. and Lee, R. T. (2006b). Local controlled intramyocardial delivery of platelet-derived growth factor improves postinfarction ventricular function without pulmonary toxicity. *Circulation* **114**, 637-644. doi:10.1161/CIRCULATIONAHA.106.639831

Ikutomo, M., Sakakima, H., Matsuda, F. and Yoshida, Y. (2014). Midkine-deficient mice delayed degeneration and regeneration after skeletal muscle injury. *Acta Histochem.* **116**, 319-326. doi:10.1016/j.acthis.2013.08.009

Ivey, M. J., Kuwabara, J. T., Pai, J. T., Moore, R. E., Sun, Z. and Tallquist, M. D. (2018). Resident fibroblast expansion during cardiac growth and remodeling. *J. Mol. Cell. Cardiol.* **114**, 161-174. doi:10.1016/j.yjmcc.2017.11.012

Kikuchi, K., Gupta, V., Wang, J., Holdway, J. E., Wills, A. A., Fang, Y. and Poss, K. D. (2011). tcf21+ epicardial cells adopt non-myocardial fates during zebrafish heart development and regeneration. *Development* **138**, 2895-2902. doi:10.1242/dev.067041

Kim, J., Wu, Q., Zhang, Y., Wiens, K. M., Huang, Y., Rubin, N., Shimada, H., Handin, R. I., Chao, M. Y., Tuan, T.-L. et al. (2010). PDGF signaling is required for epicardial function and blood vessel formation in regenerating zebrafish hearts. *Proc. Natl. Acad. Sci. USA* **107**, 17206-17210. doi:10.1073/pnas.0915016107

Kok, F. O., Shin, M., Ni, C.-W., Gupta, A., Grosse, A. S., Van Impel, A., Kirchmaier, B. C., Peterson-Maduro, J., Kourkoulis, G., Male, I. et al. (2015). Reverse genetic screening reveals poor correlation between morpholino-induced and mutant phenotypes in zebrafish. *Dev. Cell* **32**, 97-108. doi:10.1016/j.devcel.2014.11.018

Lawson, N. D. and Weinstein, B. M. (2002). In vivo imaging of embryonic vascular development using transgenic zebrafish. *Dev. Biol.* **248**, 307-318. doi:10.1006/dbio.2002.0711

Lien, C.-L., Schebesta, M., Makino, S., Weber, G. J. and Keating, M. T. (2006). Gene expression analysis of zebrafish heart regeneration. *PLoS Biol.* **4**, e260. doi:10.1371/journal.pbio.0040260

Lindahl, P., Johansson, B. R., Leveen, P. and Betsholtz, C. (1997). Pericyte loss and microaneurysm formation in PDGF-B-deficient mice. *Science* **277**, 242-245. doi:10.1126/science.277.5323.242

Lindblom, P., Gerhardt, H., Liebner, S., Abramsson, A., Enge, M., Hellstrom, M., Backstrom, G., Fredriksson, S., Landegren, U., Nystrom, H. C. et al. (2003). Endothelial PDGF-B retention is required for proper investment of pericytes in the microvessel wall. *Genes Dev.* **17**, 1835-1840. doi:10.1101/gad.266803

Marin-Juez, R., Marass, M., Gauvrit, S., Rossi, A., Lai, S.-L., Materna, S. C., Black, B. L. and Stainier, D. Y. R. (2016). Fast revascularization of the injured area is essential to support zebrafish heart regeneration. *Proc. Natl. Acad. Sci. USA* **113**, 11237-11242. doi:10.1073/pnas.1605431113

Mellgren, A. M., Smith, C. L., Olsen, G. S., Eskiocak, B., Zhou, B., Kazi, M. N., Ruiz, F. R., Pu, W. T. and Tallquist, M. D. (2008). Platelet-derived growth factor receptor beta signaling is required for efficient epicardial cell migration and development of two distinct coronary vascular smooth muscle cell populations. *Circ. Res.* **103**, 1393-1401. doi:10.1161/CIRCRESAHA.108.176768

Missinato, M. A., Tobita, K., Romano, N., Carroll, J. A. and Tsang, M. (2015). Extracellular component hyaluronic acid and its receptor Hmmr are required for epicardial EMT during heart regeneration. *Cardiovasc. Res.* **107**, 487-498. doi:10.1093/cvr/cvv190

Mosimann, C., Kaufman, C. K., Li, P., Pugach, E. K., Tamplin, O. J. and Zon, L. I. (2011). Ubiquitous transgene expression and Cre-based recombination driven by the ubiquitin promoter in zebrafish. *Development* **138**, 169-177. doi:10.1242/dev.059345

Nagashima, M., D'cruz, T. S., Danku, A. E., Hesse, D., Sifuentes, C., Raymond, P. A. and Hitchcock, P. F. (2020). Midkine-a is required for cell cycle progression of Muller Glia during neuronal regeneration in the vertebrate retina. *J. Neurosci.* **40**, 1232-1247. doi:10.1523/JNEUROSCI.1675-19.2019

Ninov, N., Borius, M. and Stainier, D. Y. R. (2012). Different levels of Notch signaling regulate quiescence, renewal and differentiation in pancreatic endocrine progenitors. *Development* **139**, 1557-1567. doi:10.1242/dev.076000

Ouyang, X., Panetta, N. J., Talbott, M. D., Payumo, A. Y., Halluin, C., Longaker, M. T. and Chen, J. K. (2017). Hyaluronic acid synthesis is required for zebrafish tail fin regeneration. *PLoS ONE* **12**, e0171898. doi:10.1371/journal.pone.0171898

Padhi, B. K., Joly, L., Tellis, P., Smith, A., Nanjappa, P., Chevrette, M., Ekker, M. and Akimenko, M.-A. (2004). Screen for genes differentially expressed during regeneration of the zebrafish caudal fin. *Dev. Dyn.* **231**, 527-541. doi:10.1002/dvdy.20153

Poss, K. D., Wilson, L. G. and Keating, M. T. (2002). Heart regeneration in zebrafish. *Science* **298**, 2188-2190. doi:10.1126/science.1077857
Pugach, E. K., Li, P., White, R. and Zon, L. (2009). Retro-orbital injection in adult zebrafish. *J. Vis. Exp.* **34**, 1645. doi:10.3791/1645
Quoseena, M., Vuppaladadium, S., Hussain, S., Banu, S., Bharathi, S. and Idris, M. M. (2020). Functional role of annexins in zebrafish caudal fin regeneration - A gene knockdown approach in regenerating tissue. *Biochimie* **175**, 125-131. doi:10.1016/j.biochi.2020.05.014
Rajan, A. M., Ma, R. C., Kocha, K. M., Zhang, D. J. and Huang, P. (2020). Dual function of perivascular fibroblasts in vascular stabilization in zebrafish. *PLoS Genet.* **16**, e1008800. doi:10.1371/journal.pgen.1008800
Rodius, S., Nazarov, P. V., Nepomuceno-Chamorro, I. A., Jeanty, C., Gonzalez-Rosa, J. M., Ibberson, M., Da Costa, R. M., Xenarios, I., Mercader, N. and Azuaje, F. (2014). Transcriptional response to cardiac injury in the zebrafish: systematic identification of genes with highly concordant activity across in vivo models. *BMC Genomics* **15**, 852. doi:10.1186/1471-2164-15-852
Sanchez-Iranzo, H., Galardi-Castilla, M., Sanz-Morejon, A., Gonzalez-Rosa, J. M., Costa, R., Ernst, A., Sainz De Aja, J., Langa, X. and Mercader, N. (2018). Transient fibrosis resolves via fibroblast inactivation in the regenerating zebrafish heart. *Proc. Natl. Acad. Sci. USA* **115**, 4188-4193. doi:10.1073/pnas.1716713115
Shih, Y.-H., Portman, D., Idrizi, F., Grosse, A. and Lawson, N. D. (2021). Integrated molecular analysis identifies a conserved pericyte gene signature in zebrafish. *Development*. **148**, dev200189. doi:10.1242/dev.200189
Smith, C. L., Baek, S. T., Sung, C. Y. and Tallquist, M. D. (2011). Epicardial-derived cell epithelial-to-mesenchymal transition and fate specification require PDGF receptor signaling. *Circ. Res.* **108**, e15-e26. doi:10.1161/CIRCRESAHA.110.235531
Stratman, A. N., Burns, M. C., Farrelly, O. M., Davis, A. E., Li, W., Pham, V. N., Castranova, D., Yano, J. J., Goddard, L. M., Nguyen, O. et al. (2020). Chemokine mediated signalling within arteries promotes vascular smooth muscle cell recruitment. *Commun. Biol.* **3**, 734. doi:10.1038/s42003-020-01462-7
Tessadori, F., Van Weerd, J. H., Burkhard, S. B., Verkerk, A. O., De Pater, E., Boukens, B. J., Vink, A., Christoffels, V. M. and Bakkers, J. (2012). Identification and functional characterization of cardiac pacemaker cells in zebrafish. *PLoS One* **7**, e47644. doi:10.1371/journal.pone.0047644
Tsai, S. L., Baselga-Garriga, C. and Melton, D. A. (2020). Midkine is a dual regulator of wound epidermis development and inflammation during the initiation of limb regeneration. *eLife* **9**, e50765. doi:10.7554/eLife.50765
Tsata, V., Mollmert, S., Schweitzer, C., Kolb, J., Mockel, C., Bohm, B., Rosso, G., Lange, C., Lesche, M., Hammer, J. et al. (2021). A switch in pdgfrb(+) cell-derived ECM composition prevents inhibitory scarring and promotes axon regeneration in the zebrafish spinal cord. *Dev. Cell* **56**, 509-524.e9. doi:10.1016/j.devcel.2020.12.009
Van Den Akker, N. M. S., Lie-Venema, H., Maas, S., Eralp, I., Deruiter, M. C., Poelmann, R. E. and Gittenberger-De Groot, A. C. (2005). Platelet-derived growth factors in the developing avian heart and maturating coronary vasculature. *Dev. Dyn.* **233**, 1579-1588. doi:10.1002/dvdy.20476
Van Den Akker, N. M. S., Winkel, L. C. J., Nisancioglu, M. H., Maas, S., Wisse, L. J., Armulik, A., Poelmann, R. E., Lie-Venema, H., Betsholtz, C. and Gittenberger-De Groot, A. C. (2008). PDGF-B signaling is important for murine cardiac development: its role in developing atrioventricular valves, coronaries, and cardiac innervation. *Dev. Dyn.* **237**, 494-503. doi:10.1002/dvdy.21436
Vanhollebeke, B., Stone, O. A., Bostaille, N., Cho, C., Zhou, Y., Maquet, E., Gauquier, A., Cabochette, P., Fukuhara, S., Mochizuki, N. et al. (2015). Tip cell-specific requirement for an atypical Gpr124- and Reck-dependent Wnt/beta-catenin pathway during brain angiogenesis. *eLife* **4**, e06489. doi:10.7554/eLife.06489
Vanlandewijck, M., He, L., Mae, M. A., Andrae, J., Ando, K., Del Gaudio, F., Nahar, K., Lebouvier, T., Lavina, B., Gouveia, L. et al. (2018). A molecular atlas of cell types and zonation in the brain vasculature. *Nature* **554**, 475-480. doi:10.1038/nature25739
Venero Galanternik, M., Castranova, D., Gore, A. V., Blewett, N. H., Jung, H. M., Stratman, A. N., Kirby, M. R., Iben, J., Miller, M. F., Kawakami, K. et al. (2017). A novel perivascular cell population in the zebrafish brain. *eLife* **6**, e24369. doi:10.7554/eLife.24369
Volz, K. S., Jacobs, A. H., Chen, H. I., Poduri, A., Mckay, A. S., Riordan, D. P., Kofler, N., Kitajewski, J., Weissman, I. and Red-Horse, K. (2015). Pericytes are progenitors for coronary artery smooth muscle. *eLife* **4**, e10036. doi:10.7554/eLife.10036
Wang, J., Karra, R., Dickson, A. L. and Poss, K. D. (2013). Fibronectin is deposited by injury-activated epicardial cells and is necessary for zebrafish heart regeneration. *Dev. Biol.* **382**, 427-435. doi:10.1016/j.ydbio.2013.08.012
Whitesell, T. R., Chrystal, P. W., Ryu, J.-R., Munsie, N., Grosse, A., French, C. R., Workentine, M. L., Li, R., Zhu, L. J., Waskiewicz, A. et al. (2019). foxc1 is required for embryonic head vascular smooth muscle differentiation in zebrafish. *Dev. Biol.* **453**, 34-47. doi:10.1016/j.ydbio.2019.06.005
Winkler, E. A., Bell, R. D. and Zlokovic, B. V. (2010). Pericyte-specific expression of PDGF beta receptor in mouse models with normal and deficient PDGF beta receptor signaling. *Mol. Neurodegener.* **5**, 32. doi:10.1186/1750-1326-5-32
Yip, J. K., Harrison, M., Villafuerte, J., Fernandez, G. E., Petersen, A. P., Lien, C.-L. and Mccain, M. L. (2020). Extended culture and imaging of normal and regenerating adult zebrafish hearts in a fluidic device. *Lab. Chip* **20**, 274-284. doi:10.1039/C9LC01044K